Auto-encoder-assisted analysis of amplitude and wavelength modulation of near-wall turbulence by outer large-scale structures in channel flow at friction Reynolds number of 5200.

L. Agostini*

Departement of Fluids, Thermal and Combustion

CNRS / Institut Pprime/ Université de Poitiers, France

M. Leschziner†

Department of Aeronautics, Imperial College London, London, UK

(Dated:)

Abstract

The present paper reports a novel methodology that allows the intensity of, and the underlying mechanism for, the amplitude and length-scale modulation (amplification or attenuation) of the turbulent stresses in the inner layer of a channel flow at $Re_\tau \approx 5200$ to be clarified. A unique aspect of the present framework is the use of an auto-encoder algorithm to separate full-volume extremely large DNS fields into large-scale and small-scale motions. This approach is adopted in preference to the empirical mode decomposition (EMD) previously used by the present authors at the lower Reynolds number, $Re_\tau \approx 1000$, because the resource requirements posed by the EMD quickly become untenable due to the extremely large direct numerical simulation (DNS) data set and the large solution box needed to capture the wide spectrum of scales at the present Reynolds number. A second original element is a formalism that derived the modulation, conditional on large-scale fluctuations, from continuous statistical quantities represented as multivariable-joint probability-density functions (*pdfs*), thus obviating the need for any discrete representation or binning beyond that imposed by the discrete DNS solution. A third novel aspect is the use of the length-scale-wise derivative of the second-order structure function to quantify the modulation (increase or decrease) in the length scale, again conditional on the large-scale structures. Apart from illuminating the modulation itself, the study examined the validity of the Quasi-Steady Hypothesis which proposes that the near-wall turbulence is universal when scaled by the spatially and temporally varying large-scale wall shear stress, rather than its time average.

I. INTRODUCTION

The notion that the local turbulent state in the near-wall region of a turbulent boundary layer is divorced from structural properties – specifically, large-scale structures – hundreds of wall units away from this region has been negated by many experimental and computational studies over the past two decades. By implication, this connection is clearly also highly pertinent to the skin friction, which presents a primary motivation for studying the subject.

One key observation, first reported in [1–3] and derived from hot-wire measurements in boundary layers up to $Re_\tau \approx 19000$, is that the near-wall turbulence is substantially per-

* lionel.agostini@univ-poitiers.fr

† mike.leschziner@imperial.ac.uk

turbed by "footprints" associated with distinctive large-scale outer structures in the log-layer region at the wall-normal distance $y^+ \approx 4\sqrt{Re_\tau}$. Around this same location, the streamwise turbulence energy is also observed to features a plateau [4, 5], or even a weak secondary peak [6] relative to the principal maximum at $y^+ \approx 12$, either of which contradicts the continuous logarithmic decline predicted by Townsend's Attached-Eddy Hypothesis [7]. An important consequence of footprinting is the amplification and attenuation of the small-scale motions effected in harmony with positive and negative large-scale fluctuations, respectively — a phenomenon referred to as "amplitude modulation". The intensity of the modulation is observed to go hand-in-hand with the intensity of the large-scale outer structures and their footprints, the latter two rising with the Reynolds number [8]. In addition, a few recent studies [9–12], discussed later, have provided evidence of "frequency modulation" – i.e., the increase and reduction in the time scale of the near-wall turbulence.

Alongside a general wish to record and understand the above interactions, interest in them is driven by three specific questions:

(i) What fundamental mechanisms drive the modulation process?

(ii) Is the near-wall turbulence – and, more specifically, its small-scale part – universal if scaled with the large-scale skin-friction, rather than with the average value?

(iii) Do the interactions have consequences to the effectiveness of control schemes designed to reduce the skin friction?

Question (ii) can also be recast as follows:

(iv) Does near-wall turbulence satisfy the quasi-steady hypothesis, wherein the small-scale turbulence responds (almost) instantaneously and linearly to the large-scale perturbations?

Statistical properties pertaining to the amplitude-modulation process have been reported, discussed and dissected in many recent papers. Experimental studies, the large majority performed with single hot-wire probes in boundary layers – e.g., [8, 11, 13–15] – cover a wide range of Reynolds numbers, extending to $Re_\tau \approx 19000$. While all provide valuable insight into many aspects of the modulation process, none addresses specifically the questions posed above, simply because of the restricted nature and volume of the data that could be

extracted experimentally. In contrast, computational studies, among them [16–21], mostly employ DNS and give access to full-volume realisations that allow the above questions to be addressed, albeit at relatively low Reynolds numbers. This route has been taken by Agostini and Leschziner [22] and Chernyshenko [23], the latter specifically in support of formulating their quasi-steady (and quasi-homogeneous) theory pertaining to question (ii) and (iv) posed above.

Agostini & Leschziner [22, 24, 25] have previously examined a variety of aspects of the above large-scale/small-scale interactions by analysing the DNS data of Touber and Leschziner [26] and Agostini and Leschziner [24] for channel flow at $Re_\tau \approx 1000$, a value for which the interactions are relatively weak, however. They did so by employing their own spatially bi-dimensional Empirical Mode Decomposition (EMD) to separate the turbulence spectrum across many full-volume DNS realisations into small, medium and large-scale modes. This allowed them to construct small-scale statistics, conditional on large-scale skin-friction footprints, so as to infer the mechanisms by which small-scale amplification by positive footprints dominate asymmetrically over small-scale attenuation by negative footprints, thus explaining the progressive rise in the perturbations of the near-wall layer by footprinting.

Of particular relevance to question (i) in the above list on the mechanisms responsible for the amplitude modulation are the recent studies by Agostini and Leschziner [22, 25, 27], the last focusing specifically on the effects of modulation on the drag-reduction effectiveness achieved by imposing oscillatory spanwise wall motion in channel flow at $Re_\tau \approx 1000$. They show that the mechanisms of amplification and attenuation are, essentially, the same in both the canonical and actuated cases, the principal element being the increase and decrease in near-wall turbulence generation provoked, respectively, by corresponding increase and decrease in the strain rate close to the wall provoked by the large-scale fluctuations. However, the effects are more pronounced in the low-drag actuated flow, in which the modulation due to negative and positive large-scale fluctuations are substantially asymmetric, implying the origin of the decline in drag-reduction effectiveness as the Reynolds number increases [28–30].

In contrast to amplitude modulation, frequency modulation has received far less attention. This rarity has provided strong impetus for one major element of the present study, wherein a statistical analysis of the second-order structure function is proposed as a basic for illuminating the modulation of the length scale of the near-wall turbulence by the foot-

prints. To the authors' knowledge, there are only four studies that focus on this type of interaction for canonical flows – namely those by Ganapathisubramani *et al.* [9], Baars *et al.* [10], Pathikonda and Christensen [11] and Iacobello *et al.* [12], the first three of which are based purely on processing experimental data, while the fourth involves both experimental and computational elements.

Ganapathisubramani *et al.* [9] examined the frequency modulation, alongside amplitude modulation, in the near-wall region of a boundary layer at $Re_\tau = 14150$ (database obtained by Nickels *et al.* [31]). They did so by counting the number of maxima and minima in the recorded small-scale signals and analysing conditional small-scale spectra, observing that frequency modulation is relatively weak, confined to $y^+ < 100$ and being positively correlated with the intensity of the large-scale motions. A limitation of the study, acknowledged explicitly therein, is that the results were observed to be sensitive to the the width of the bins used to separate samples of the large-scale motions as a basis of the conditional characterisation of the modulation.

Baars *et al.* [10] analysed hot-wire signals of the streamwise velocity in the same boundary layer that considered by Ganapathisubramani *et al.* [9] but chose to use wavelet transforms so as to extract the amplitude and frequency modulation simultaneously. The outcome was in the form of time shifts between large-scale motions and amplitude and frequency variations in the small scales. In essence, these results confirmed the conclusions derived by Ganapathisubramani *et al.* [9], including the observation that frequency modulation was weaker than amplitude modulation. However, significant uncertainties arise from the sizeable sensitivity of the frequency modulation to the choice of the wavelet shapes forming the basis of the analysis. Following Baars *et al*'s wavelet-based methodology, Pathikonda and Christensen [11] analysed the streamwise and wall-normal velocity fields in a boundary layer in a water channel at $Re_\tau \approx 1400$, arriving at similar conclusions in respect of the frequency modulation being only significant within $y^+ < 100$.

Iacobello *et al.* [12] applied the so-called Natural Visibility Graph (NVG) approach, developed by Lacasa *et al.* [32], to the boundary layer at $Re_\tau \approx 14750$, previously examined in [9, 10], and to the channel flow of at $Re_\tau \approx 5200$ [33]. The principle of this method is to count how many times a signal at a point (a "node") can be linked to other discrete values by straight lines without crossing any other parts of the signal. The shorter the wavelength is, the fewer connections there are, while the reverse applies to longer wavelengths. As part

of their study, Iacobello *et al.* [12] investigated the validity of the quasi-steady hypothesis by relating the velocity-fluctuations signals at $y^+ \approx 10$ to the large-scale streamwise velocity derived from Fourier-based filtering. To this end, they estimated the frequency of various signal subsets for all three velocity components conditioned on bins of large-scale skin-friction values, and they show that only the streamwise signal complies with the quasi-steady scaling laws. Limitations of the method include rising uncertainties of the inter-node counting process at large wavelength and the non-transparent relationship between the counting formalism and the continuous power spectra of the signals being processed.

Contrasting with the previous studies on frequency modulation outlined above, the present paper sets out a methodology that distinguishes itself by a clear and transparent formalism that rests on processing continuous statistical quantities - joint PDFs and the structure function, in particular - and which does not require any discrete representation or binning beyond that imposed by the discrete DNS solution at $Re_\tau \approx 5200$. A unique aspect of the present framework is the use of an auto-encoder algorithm to separate full-volume DNS realisations into large-scale and small-scale motions. This approach is adopted in preference to the EMD previously used by the present authors at the lower Reynolds number $Re_\tau \approx 1000$, because the resource requirements posed by the EMD quickly become untenable due to extremely large DNS data set and the large solution box needed to capture the wide spectrum of scales at the higher Reynolds number.

The present paper deals specifically with four aspects :

(1) the manner in which the decoder-encoder model is used to separate the scales over full- volume DNS realisations;

(2) the method by which insightful conditional statistics are derived from the separated fields;

(3) the manner in which the statistics under (2) provide insight into the mechanisms by which the large scales affect the turbulent stresses, including the small-scale portions, in terms of both amplitude and length-scale (or wavelength) modulation, the latter distinct from frequency modulation;

(4) the manner in which the decomposition under (1) allows the quasi-steady hypothesis to be tested in respect of both amplitude and length-scale modulation - i.e., the propo-

sition that the turbulence fields are universal when scaled with the instantaneous and local large-scale wall shear stress.

II. LARGE-SCALE / SMALL-SCALE SEPARATION

As noted earlier, the EMD becomes untenable at the present Reynolds number. In our previous studies, at $Re_\tau \approx 1000$, the size of the snapshot which could be post-processed by the EMD was large enough for the large-scale motions to be well defined. At $Re_\tau \approx 5200$, the ratio between small and large scales is much larger, and the size of the snapshot that needs to be accommodated for capturing the full spectrum of eddy increases dramatically. Hence, the resources needed to process full snapshots become untenable, and the EMD has to be applied to much smaller subsets in which only a small portion of the large-scale motion is contained. A disadvantage of this approach, apart from the resource issue, is that it results in a patch-wise variability of the decomposition and an ambiguity in the definition of what constitutes the large scales. Thus, an alternative data-driven methodology, referred to as "Auto-Encoder" (AE), has been adopted herein to separate the large-scale from small-scale motions.

The exploitation of AE technology in fluid mechanics is relatively recent, and it has been applied successfully as an aid to flow prediction and the analysis of turbulence physics [34, 35]. However, it is not the purpose of this paper to provide a review of the various strands of AE applications; interested readers may wish to refer to a broad description and discussion in [36] of AE techniques as pertinent to fluid dynamics.

An AE is an unsupervised machine-learning (ML) algorithm that is trained to reconstruct a representation of its inputs from a data set that is highly reduced in volume and detail relative to the full input. As illustrated in figure 1, an AE has three parts: an encoder, a bottleneck (latent space), and a decoder. Depending on how its architecture is defined, an AE can served different purposes, functioning as denoisor [37], anomaly detector [38], and estimators [39], for example. In the present study, the goal is to use the AE's ability to efficiently learn the most important features associated with large-scale outer-flow structures in a pre-defined portion of the flow and to extract them from the fields in other parts of the flow. The AE is thus used as an outer-flow-structure filter that yields a lower-order representation of raw fluctuation field. To do so, raw streamwise velocity fields at the wall-

normal location $y^+ = 4\sqrt{Re_\tau} \approx 280$, a location at which the structures are especially well defined according to Mathis *et al.* [3], are fed to the AE. The fields consist of randomly chosen subsets with size 1280×1280 data items, each being $1/48^{th}$ of the total data items in the plane. Subsets from seven DNS snapshots are used for this training, and subsets from three other snapshots are used for validation. Here, it is important to point out that the input of data in subsets is not equivalent to the patch-wise application of the EMD, discussed earlier. In contrast to the EMD, the AE learns from the entire collection of subsets, updating its knowledge of what constitutes the large-scale features for every subset fed into it. One further advantage of the AE is that it learns to forget information which is not statistically relevant – e.g., unusually large, rare, ejections or sweeps. This is an advantage over the EMD or FFT-based methods, as it ensures that the distorting effects of statistically irrelevant events in the restricted patches are suppressed or avoided altogether.

To force the AE to learn the most important features, the information passing through the AE is drastically reduced by using a relatively narrow bottleneck. The information between the input and the bottleneck is progressively reduced by using several convolutional layers, helping the AE to gradually define which features are the most important by minimising the absolute value of the reconstruction error ($J = \sum_{i=1,j=1}^{1280,1280} (output(x_i, z_j) - input(x_i, z_j))^2$), so-called Mean Squared Error (MSE), steering the AE towards reconstructing the most energetic scales, which correspond to large-scale motions in this case AE can be regarded as a generalisation of the POD [40, 41]. Both encoder and decoder have six convolution layers. Each layer contains two activation maps, and each is followed by a down-sampling layer for the encoder, or is preceded by an up-sampling layer for the decoder, the function 'exponential linear unit' (elu) [42] is used as the activation function. To avoid over-fitting, a Gaussian-noise layer and batch-normalisation layers are added to the AE's architecture during the training [43].

In the current AE architecture, the encoder has 6 convolutional layers with two filters, each followed by a subsampling layer (maxpooling). This architecture leads to a dramatic reduction in information: input images are compressed by a factor 1/2048, from a size of 1280×1280 data points to $20 \times 20 \times 2$ points in the latent space (Bottleneck). Thus, only 0.05% of the original information is available to the decoder for constructing a reduced-order version of the original input that preserves the energetic LS structures present in the original.

Initially, the AE is trained to learn only the features associated with the outer-flow structures – i.e., the data used for training are streamwise-velocity-fluctuation fields at the wall-normal location $y^+ \approx 280$. By reducing the amount of information passing through the AE's bottleneck, the AE must learn the most significant features of the input so that the output image is as close as possible to the input image. The level of closeness is defined by the absolute value of the reconstruction error J. Once the training (learning) is achieved – here done by feeding in sub-domains of size 1280×1280 wall units, chosen randomly from seven DNS 2D fields at $y^+ \approx 280$ – the AE will only use the "library" of features learned at $y^+ \approx 280$, from the streamwise velocity fields, for reconstructing all velocity components of the flow at any wall-normal plane. In this way, the large-scale motions associated with the outer-flow structures are extracted by the AE from the raw data at each and every wall-normal location. The outcome of the above process is illustrated — arguably verified, if only in a qualitative sense – in two ways. First, figures 2 and 3, show fields decomposition, spectra and streamwise energy profiles for the large-scale and small-scale motions respectively. Second, figure 4 compares the AE-generated decomposition with the more conventional empirical-model decomposition (BEMD) applied in previous studies by Agostini and Leschziner [22, 24] of channel flow at $Re_\tau = 1000$. Figure 2 shows sub-domains of streamwise-fluctuations fields across the wall-normal planes $y^+ \approx 280$ and and $y^+ \approx 12$ on the left-hand side and right-hand side, respectively, both covering the sub-domain $x^+ \times z^+ \approx 16000 \times 8000$, corresponding to 1/8 and 1/6 of the total computational-box dimensions, respectively. The plots, from top to bottom, are for the full streamwise-fluctuations fields, the large-scale motions and the residual small-scale fields. Specific feature that deserve to be underlined are, first, the strong dominance of the large-scale component at the outer location; second, the presence of large-scale footprints in the near-wall layer; third, the fine-grained small-scale features in the near-wall layer; and fourth the influence of the large-scale footprints on the intensity of the small-scale structures in the near-wall layer.

Figure 3 demonstrates the scale-separation process by way of pre-multiplied energy-density spectra, in the $y^+ - \lambda_z^+$ (spanwise wavelength) plane for – top to bottom rows – the streamwise, wall-normal and spanwise components, respectively. The red contours identify the large scales, while the blue contours pertain to the small scales, the sum of the two being identified by the black contours. The corresponding energy profiles in the wall-normal direction are given in the middle column, while the plots on the right-hand-side plots show

the spectra with the energy density normalised by the total-energy profiles given in the middle column. The purpose of including the last set of plots is to bring out more clearly the proportion of large-scale and small-scale energy density in regions in which the magnitude of the energy is low. The plots convey a well-defined scale separation, with the large scales confined to wavelength values $\lambda_z^+ > 800$, which compares to $\lambda_z^+ \approx 100$ at which the streamwise energy density peaks at $y^+ \approx 13$. The normalised spectra for the streamwise fluctuations also bring out prominently the penetration of the large-scale energy right down to the wall. This penetration, as well as the high level of large-scale energy, relative to the respective total levels, is further brought out in the energy-profile plots. An interesting observation is the exceptionally high anisotropy in the large-scale stress components, implied by the precipitous decline in the wall-normal stress towards the wall. One facet of this behaviour is that small-scale structures tend to be more isotropic than large-scale eddies. Another aspect arises from the large-scale/small-scale analysis reported by Agostini and Leschziner [22, 24, 25] for channel flow at $Re_\tau \approx 1000$, which strongly suggests that footprinting is closely associated with large-scale sweeps, ejection and quasi-steady streamwise vortices. Specifically, sweeps result in "splatting" due to inviscid wall blocking and the enhanced transfer of energy from the wall-normal component to the wall-parallel directions.

Next, figure 4 provides some comparisons between the AE- and BEMD-derived decompositions. Here, it needs to be reiterated that the BEMD is too resource-intensive to be used across the entire solution domain. For this reason, the comparisons shown in figure 4 restrict themselves to two partial y-planes of size $x^+ \times z^+ = 16000 \times 8000$ containing 1280×1280 data points within one DNS realisation. The BEMD is a purely data-driven method, wherein the LS filter characteristics are defined directly from the snapshot. Hence, if the snapshot is not large enough to capture the full length-scale range of the structures populating the flow, the LS filter will be slightly different from snapshot to snapshot, which is one further resource-related limitation of the use of the BEMD for the present Reynolds number. In agreement with earlier studies in [22, 24], the BEMD is used to decompose the spectrum into 5 modes, each encapsulating a narrow range of length scales. Also, as done before, the upper two modes (strictly mode 4 and the residual) are defined as representing the large-scale portion of the spectrum. In figure 4, the two images in the top row show the raw data at $y^+ = 280$ and 12, respectively, while the second and third rows convey the decomposition returned by the AE and BEMD, respectively. While this visual representation is essentially qualitative

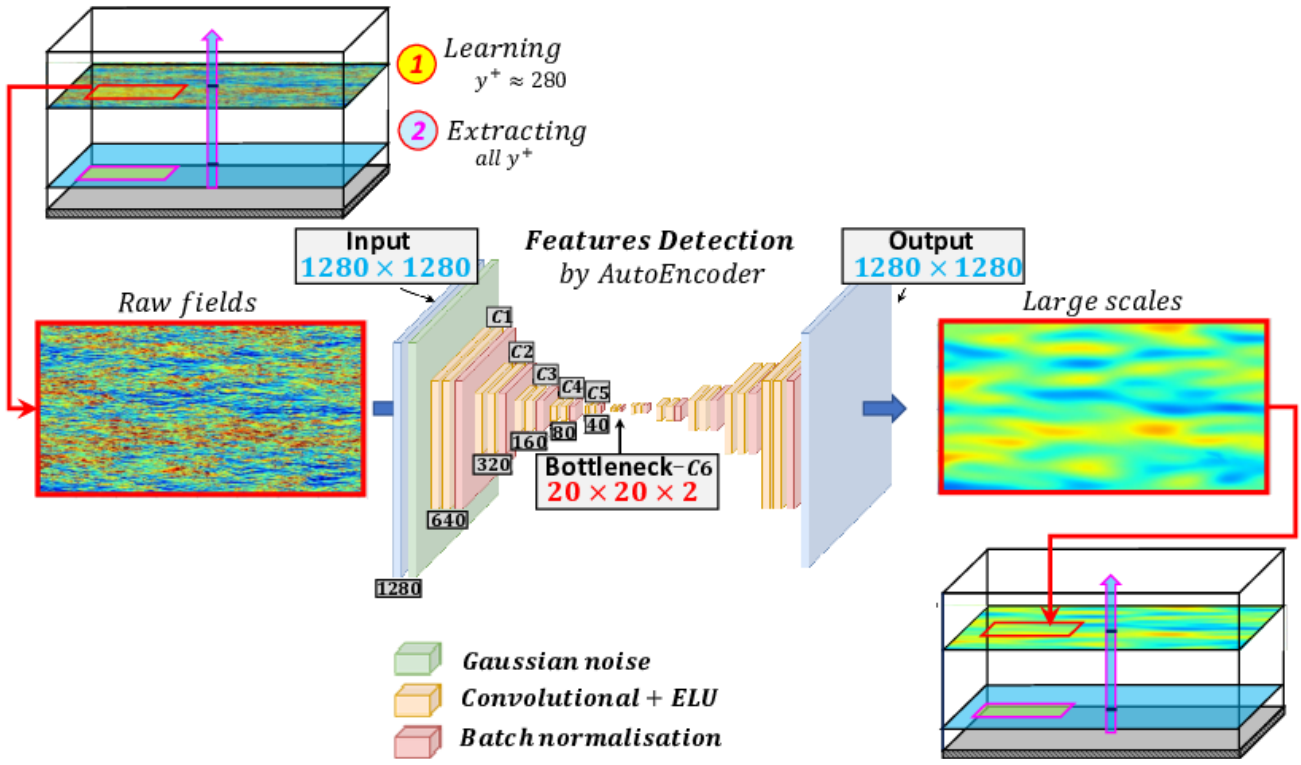

FIG. 1: Schematic representation of the process of extracting the large-scale motions by using a multi-layer Auto-Encoder. Patches on the plane $y^+ \approx 280$ are 8×6 sub-domains (in x and z directions, respectively) of size $\Delta x^+ \approx 1280$ and $\Delta z^+ = 1280$ used for the learning process.

in nature, it demonstrates strong similarities of the large scales LS derived from both methods. The raw field at $y^+ \approx 12$, figure 4(b), shows clearly the modulation of the small-scale motions by the outer-flow structures, and figures 4(d) and 4(f) convey qualitatively the fact this modulation is correlated with the the large scales extracted by using either the AE or the BEMD. It is important to recall here that the AE is only trained at $y^+ \approx 280$. While both reconstructions at $y^+ = 12$ are very similar, the AE-based decomposition seems to provide LS structures that are more continuously correlated in the streamwise direction, which complies better with the expectation of streamwise-coherent LS regions.

The scale separation process – specifically, the wavelength separating the small scales from the large scales - is influenced by the AE architecture – in particular, the number of convolutional layers, the number of down-sampling layers and the number of filters used for each convolutional layer. As indicated in Fig.1, the AE configuration used in this study

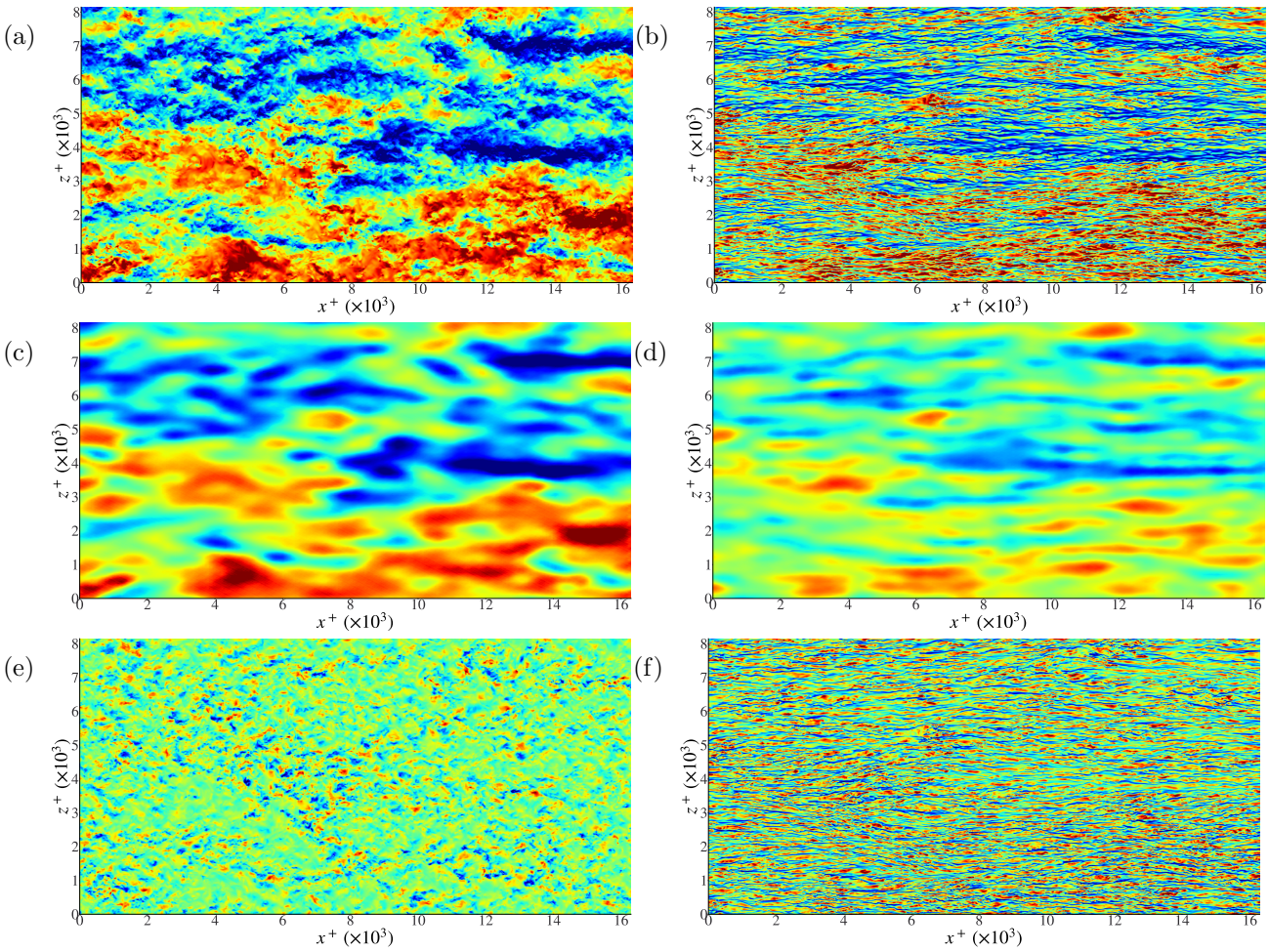

FIG. 2: Illustration of scale decomposition using the approach shown in Fig. 1 at two wall-normal locations over a portion of the $x-z$ DNS box (1/8th in streamwise direction and 1/6th in streamwise direction); (a),(c),(e): $y^+ \approx 280$; (b),(d),(f): $y^+ \approx 13$; (a),(b): full streamwise-fluctuations fields (input to the auto-encoder); (c),(d): large-scale fluctuations fields (output of the auto-encoder); (e),(f): small-scale fluctuations (total minus large-scale fluctuations).

features twelve convolutional layers, each containing two filters, the sixth layer being the bottleneck. The sensitivity of the scale separation to the number of filters is investigated by varying the filter number in the bottleneck within the range 1 to 8, resulting in the decoder having access, correspondingly, to between 0.025% and 0.200% of the original information. This sensitivity is conveyed in Fig. 5(a) and (b), which shows spanwise spectra at $y^+ = 280$ and 12, respectively, N being the number of filters. In accord with the full spectral map in Fig.3(a), the energy in the outer region is dominated by the large scales, while in the

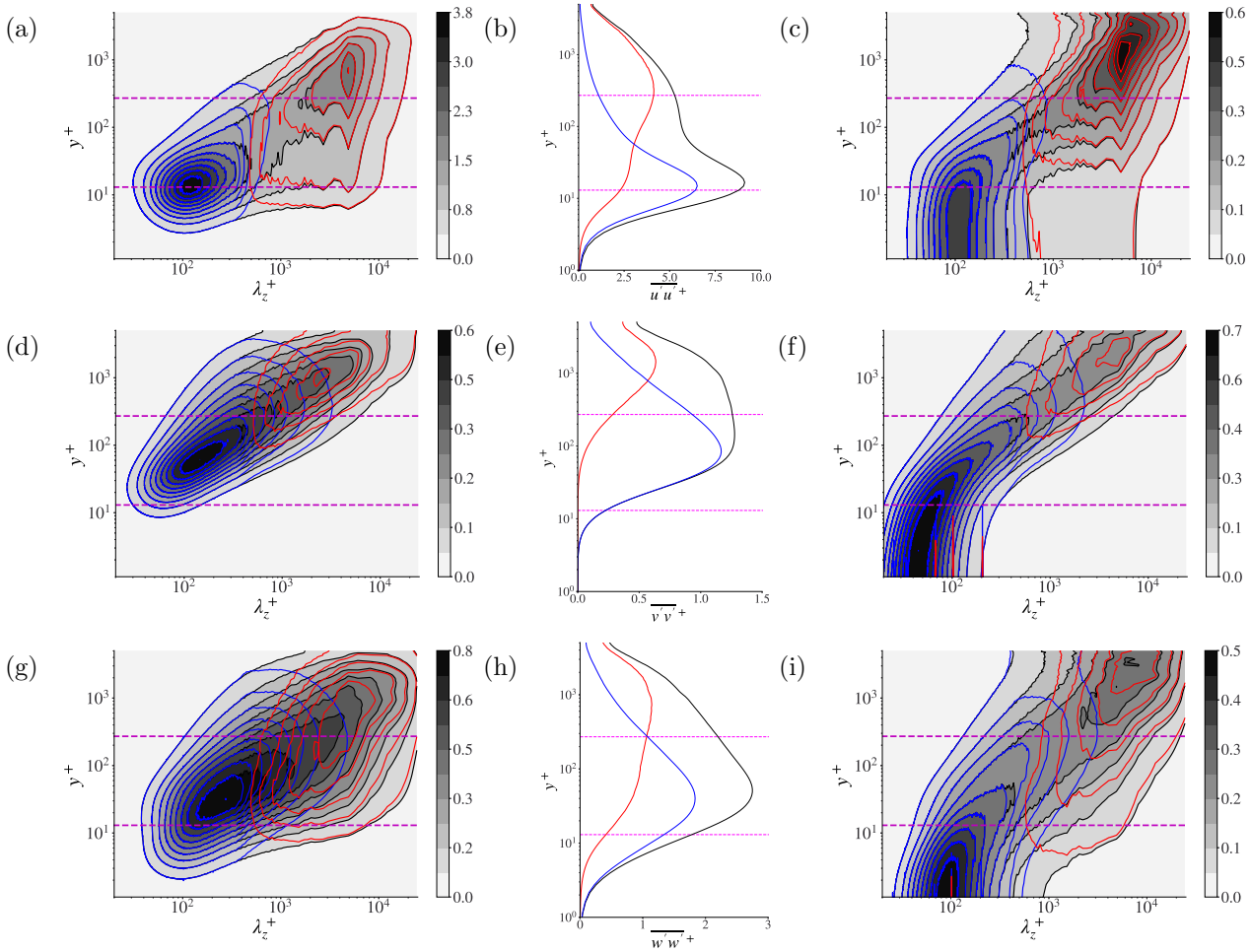

FIG. 3: Statistical properties of small-scale and large-scale fluctuations in (a),(b),(c) streamwise, (d),(e),(f) wall-normal and (g),(h),(i) spanwise directions, respectively; (a),(d),(g): premultiplied power spectra – black contours identify total fluctuations, red contours large-scale fluctuations, blue contours small-scale fluctuations; (b),(e),(h): corresponding streamwise-energy profiles (colour code same as in LHS column); (c),(f),(i): premultiplied power spectra normalised by the total energy (black) profiles in the middle column.

near-wall region the energy peaks at $\lambda_z^+ \approx 100$, signifying the separation distance of the streaks. The energy level of the large scales in the near-wall region is around 40% of that in the outer region, and this is in agreement with the y^+-wise decline towards the wall seen in Fig.3(a) around $\lambda_z^+ = 5000 - 8000$. As the number of bottleneck filters rises, the

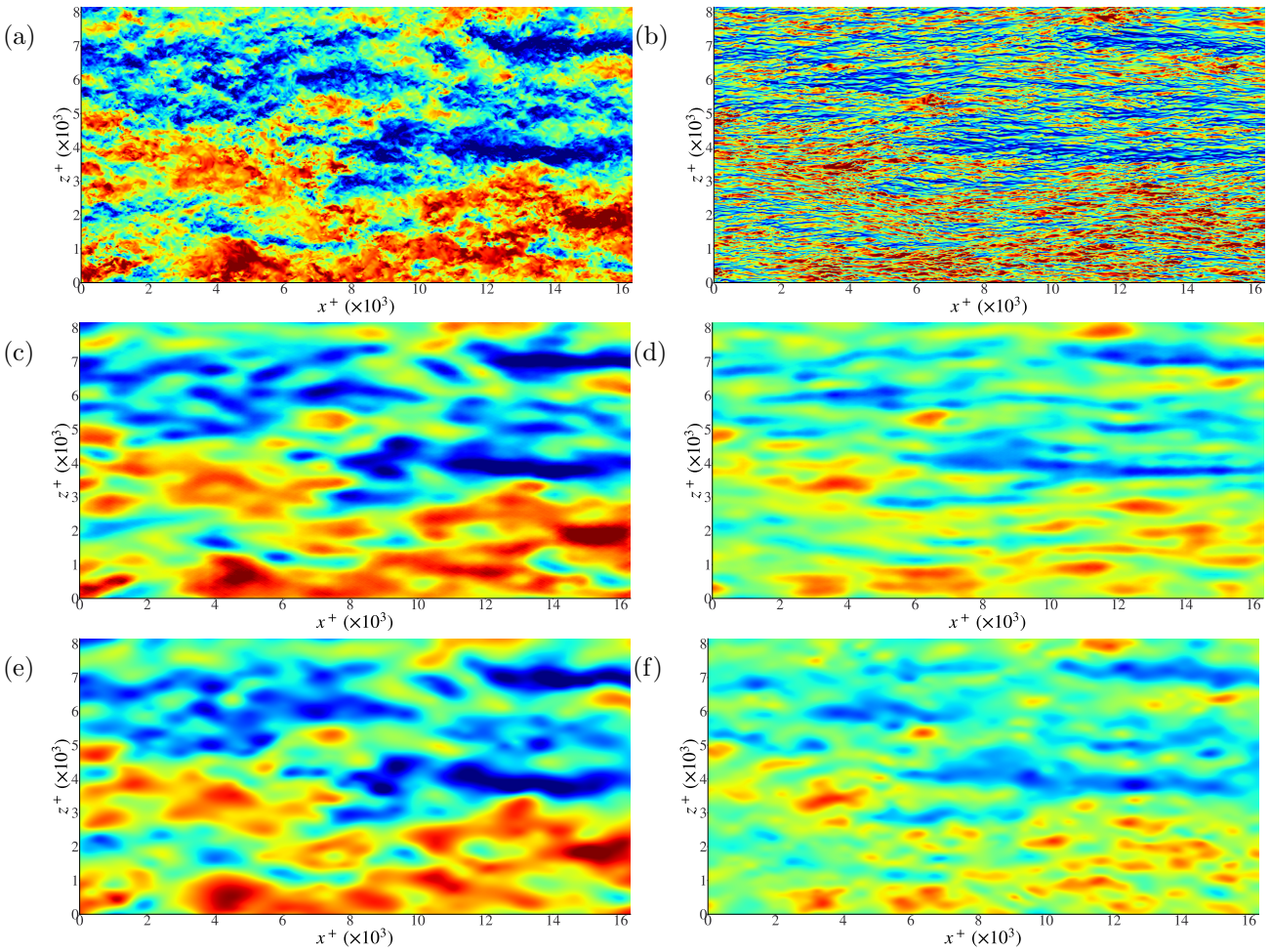

FIG. 4: Extraction of large-scale fluctuations at $y^+ \approx 280$ (left column) and $y^+ \approx 12$ (right column) using Auto-Encoder (c,d) and bi-dimensional empirical mode decomposition (e,f).

quantity of information passing through the AE bottleneck increases, manifesting itself by the AE output gradually encroaching upon the upper range of the low-wavelength scales, thus resulting in a shift of the small-scale/large-scale boundary from $\lambda_z^+ \approx 1000$ to ≈ 500. This sensitivity clearly introduces a level of ambiguity into the scale-separation process. However, this ambiguity is no different from that in any other scale-separation practice – the simplest being an arbitrary choice of a hard wavelength low-pass/high-pass filter or decisions on the attribution of EMD modes to the large-scale, intermediate-scale and small-scale subranges. For the statistical analysis to follow, the choice has been made to use two filters ($N = 2$), separating the large from the small scales at $\lambda_z^+ \approx 700$. This value places the mean separation wavelength roughly in the middle of the spectral map in Fig.3(b) within the region separating the small-scale and large-scale energy peaks. In any event, it

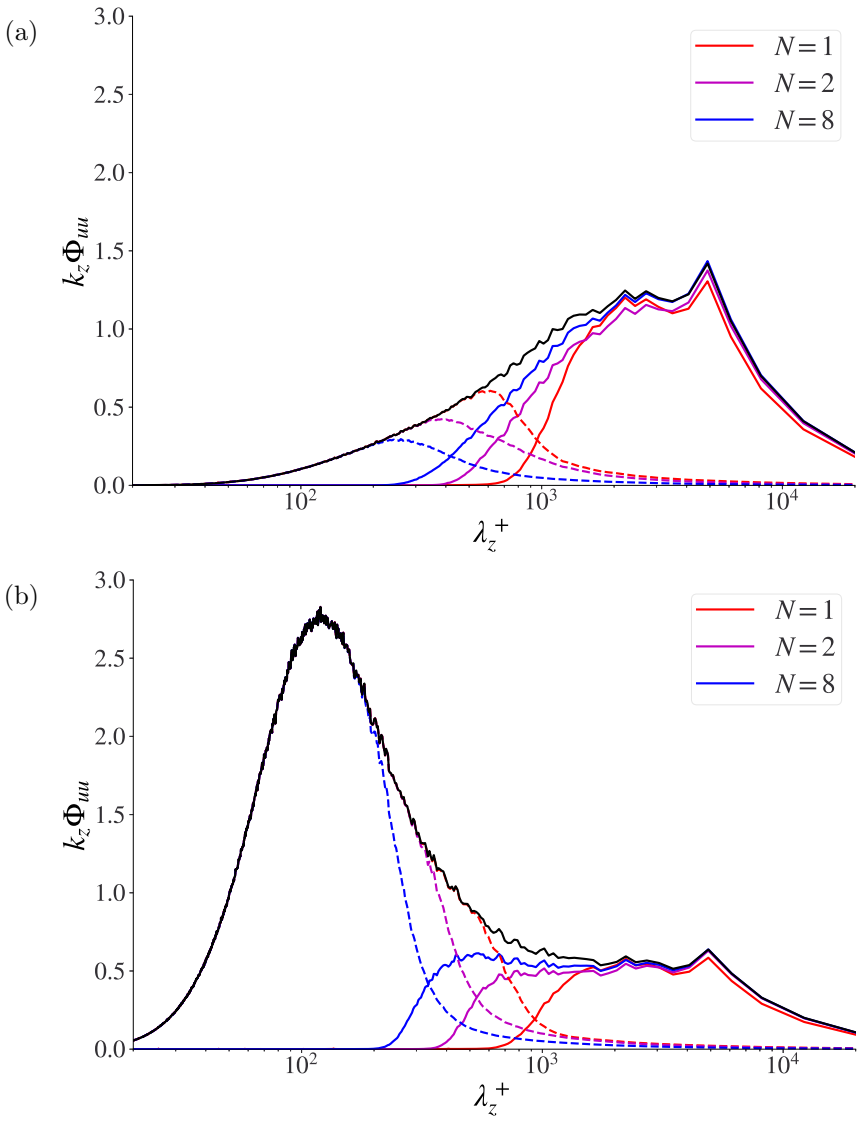

FIG. 5: Sensitivity of the small-scale/large-scale separation process to the number of filters used in AE bottleneck; power spectral density of the AE output for the streamwise-velocity fluctuations at (a) $y^+ = 280$ and (b) $y^+ = 12$.

is important to underline the fact that the precise scale-separation wavelength, within the limits considered above, has no material consequence to the physical interpretations that follow below.

III. STATISTICAL CHARACTERISATION

A. Amplitude modulation

Although the principal purpose of this study is to examine length-scale modulation by way of the second-order structure function, it is appropriate and natural to link it to earlier studies on amplitude modulation by Agostini and Leschziner [22, 25]. The relevant statistical processing is introduced here first, in a condensed form, to provide an essential background necessary for understanding some results reported below on amplitude modulation. The justification for including considerations on amplitude modulation rests on three arguments: first, key parts of the particular statistical-processing methodology applied to the length-scale modulation have been defined by reference to amplitude modulation. Second, previous conclusions arose from DNS data at the much lower Reynolds number $Re_\tau \approx 1000$. Third, the present practice of large-scale/small-scale separation is quite different from the previous EMD method.

A key aspect of the present statistical-processing method is to derive all statistical quantities from the general joint PDF $P(X_1, ..., X_n, Y)$ in which X_i identify any flow property derived from the DNS – e.g., velocity fluctuations – and Y identifies a conditional variable upon which the statistics of X_i are assembled. In the context of examining amplitude modulation, Agostini and Leschziner examined a range of conditional statistics [22, 25, 27], the two most important of which arise from the joint PDF and the PDF of the conditional variable $P(Y)$, as derived from:

$$\overline{X_i}|_Y = \int_{-\infty}^{+\infty} \cdots \int_{-\infty}^{+\infty} X_i \frac{P(X_1, ..., X_n, Y)}{P(Y)} dX_1 ... dX_n \tag{1}$$

$$\begin{aligned} \overline{x_i' x_j'}|_Y &= \overline{(X_i - \overline{X_i}|_Y)(X_j - \overline{X_j}|_Y)}|_Y \\ &= \overline{X_i X_j}|_Y - \overline{X_i}|_Y \, \overline{X_j}|_Y, \end{aligned} \tag{2}$$

where Y is chosen to be Cf_{LS}, representing the unsteady and locally varying skin friction induced by the footprints of the large-scale motions. The merit of these conditional values is that they bring out the influence of large-scale fluctuations on the quantities considered at large positive and negative Cf_{LS} values without the obscuring influence, or weighting,

of the low-density levels in $P(Cf_{LS})$. Other statistics can then be derived from the above two, an example being the conditional production rates derived from products of the second moments and the conditional strain rate – e.g., $\left[-\overline{u'v'}dU/dy\right]|_{Cf_{LS}}$ shown in figure 11. Any of these statistical properties can then be conveyed by respective fields in $y^+ - Cf_{LS}$ plane, because of the x, z-wise homogeneity of the statistical properties, subject to the lag between the large-scale Cf_{LS} fluctuations and the large-scale velocity fluctuations u_{LS} at any y^+ value being removed.

B. Length-scale modulation

The second-order structure function is proposed herein as a basis for investigating length-scale modulation. Given the fields of velocity $u(x, z)$ across any y-plane, and the large-scale skin-friction $Cf_{LS}(x, z)$, the latter being wall footprint of the outer-large scale structures shifted forwards in streamwise direction by $\Delta x = \Delta y \tan\theta$, with $\theta \approx 11^o$ (see justification to follow towards the end of this section), the starting point is the derivation of the PDFs from the DNS data set in which $s_{u,\delta z} = u(x, z + \delta z) - u(x, z)$ is the instantaneous difference between velocity fluctuations separated by a given (i.e. chosen) value δz (the subscript y is omitted henceforth).

The n^{th} order structure function (S^n) for a given δz can be derived from:

$$S_u^n(\delta z) = \langle |u(x, z + \delta z) - u(x, z)|^n \rangle = \int s_{u,\delta z}^n P(s_{u,\delta z}) ds_{u,\delta z} \tag{3}$$

The representation of the structure function via its PDF is important in the context of, and is consistent with, the strategy of using the multi-variable joint PDF strategy, as expressed by equation (1).

Here, the focus is on the second-order structure function, or rather its incremental derivative with respect to δz, used as the surrogate of the scale-wise distribution of the energy. As demonstrated by Davidson *et al.* [44] and Agostini and Leschziner [45] , there is a close relationship between the energy spectra and the derivative of the structure function, as is exemplified by figures 6a and 6b for the total streamwise-fluctuation field.

There are several advantages that motivate the present use of the structure function. One lies in the fact that it is a purely data-driven method, the results of which do not depend upon a projection basis and on how the hyper parameters are tuned, as is the case

for FFT and wavelet-based analyses (window size, window function, etc. see [46]). A second advantage is that the signal does not need to be continuous – for example, in the case of a signal with one harmonic which contains several periods but with parts of signal missing, this would cause serious difficulties for a FFT-based approach. A third advantage relates to the conditional nature of the statistics that form the basis for identifying the dependence of the length scale on Cf_{LS}. As the conditional statistics are derived from the *joint pdf* of the structure function, the conditional wavelength can be determined without any specific constrains on the length of the input signal, as this latter can continuously vary with the value of Cf_{LS}. Finally, the structure function can be determined reliably for long wave lengths for which the signal is not represented by a full wave. This allows the contribution of the largest scales resolved by the DNS to be represented much more accurately that via the spectra, which suffer from limitation imposed by the FFT when the sample of scales is sparse and the domain size limited. As will emerge below, length-scale shifts in this derivative will be used to identify length-scale modulation conditional on Cf_{LS}.

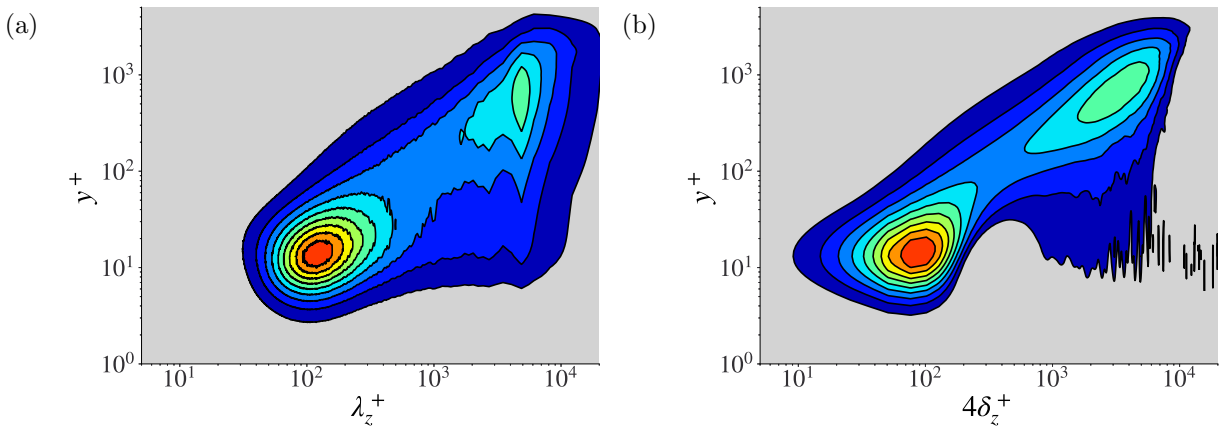

FIG. 6: Equivalence between (a) premultiplied energy spectra and (b) premutiplied derivative of second-order structure function. Both maps consolidate the full data set for the streamwise fluctuations.

By using the multi-variable PDF approach, the variation of the structure function and its derivative conditional on Cf_{LS} can be investigated in the same sense as previously undertaken in relation to amplitude modulation, by way of:

$$S_u^n(\delta z) = \iint s_{u,\delta z}^n P(s_{u,\delta z}, Cf_{LS}) ds_{u,\delta z} dCf_{LS} \tag{4}$$

$$S_u^n(\delta z)|_{Cf_{LS}} = \int s_{u,\delta z}^n \frac{P(s_{u,\delta z}, Cf_{LS})}{P(Cf_{LS})} ds_{u,\delta z} \tag{5}$$

With the joint PDF, $P(s_{u,\delta z}, Cf_{LS})$, derived separately for each and every computational y place and for a set of values δz, the second-order structure function conditional on Cf_{LS} can be derived using equation (5) with $n = 2$. Alongside, the conditional structure function $S_u^2(\delta z)|_{Cf_{LS}}$, its premultiplied derivative $\delta z \frac{dS_u^2(\delta z)}{d\delta z}|_{Cf_{LS}}$ can be computed at every wall-normal location. It is this derivative on which attention focuses primarily. Again, the reason is that the variation of this variable across δz is closely connected to the energy-density spectrum $\Phi_{uu}(\lambda_z)$, with λ_z connected to the separation δz, as is discussed at length in [45].

A limitation posed by equations (4) and (5) arises from the fact that the separation δz causes the two fluctuations $u(x, z)$ and $u(x, z + \delta z)$ to be located at different values of Cf_{LS}. However, in practice the spatial variation of Cf_{LS} is modest within the range of δz of interest and of thus of little effect on the contribution of the difference $u(x, z + \delta z) - u(x, z)$ to the $P(s_{u,\delta z}, Cf_{LS})$ distributions. Tests with excluding samples of this difference when the variation in Cf_{LS} exceeds prescribed limits have been performed by using a limiter W given by equation (6), where only samples satisfying the relation $W > \alpha$ were retained, as expressed by equation (7):

$$W = \frac{2 \times Cf_{LS}(x, z + \delta z) \times Cf_{LS}(x, z)}{(Cf_{LS}(x, z + \delta z))^2 + (Cf_{LS}(x, z))^2} \tag{6}$$

$$Cf_{LS} \Leftarrow \frac{Cf_{LS}(x, z + \delta z) + Cf_{LS}(x, z)}{2}|_{W>\alpha} \tag{7}$$

Use of different values of α, ranging from 0 to 0.995, was observed to have insignificant consequences to the interpretation of the results.

A feature of the above conditional statistics that hinders an unambiguous interpretation of the modulation process is that field of u_{LS} is different at different y^+ locations. The objective here is, however, to examine statistics that are conditional on a single reference field. This reference field is chosen to be Cf_{LS}. This allows questions to be asked about the validity of the quasi-steady concept which hypothesizes that scaling the wall-normal small-scale turbulence properties with the local large-scale wall shear stress $\tau_{w,LS}$ results in identical statistics, i.e. statistics that do not vary with Cf_{LS}. However, a question that needs to be addressed is whether the condition Cf_{LS} is equivalent to the condition $u_{LS}(y^+)$.

This equivalence is substantially favoured by the fact that large-scale fluctuations are highly correlated in y^+, subject to a spatial streamwise lag, as is discussed by Hutchins *et al.* [2] and several other studies. This has also been found to be the case in the present data set. Hence, here, the assumption has been invoked that u_{LS} is represented by Cf_{LS}, subject to the spatial lag $\Delta x^+ = \Delta y^+ / \tan(\theta)$, with the angle arising from the two-point correlation maps. A consequence of this lag, and thus the gradient in u_{LS}, is a degree of ambiguity as regards the derivative of $S(\delta z)$, which is conditional of u_{LS} – or rather its Cf_{LS} equivalent. This is a problem similar to that discussed earlier in relation to spanwise variations in u_{LS}. However, the lag between two neighbouring y^+ planes is small and the effect on the statistics is thus negligible.

C. Quasi-steady hypothesis

One objective of the present study is to investigate whether the quasi-steady hypothesis (QSH) applies in respect of amplitude as well as length-scale modulation, the former investigated by Agostini and Leschziner [22] for $Re_\tau \approx 1000$. In essence, the QSH states that the small-scale turbulence statistics, when normalised by the local and instantaneous large-scale friction velocity, are universal – i.e., independent of the large-scale fluctuations. Such a behaviour implies that the turbulence state adjusts itself rapidly to perturbations provoked by the large-scale motion, or that the time scale governing small-scale mechanisms is much shorter than the time scale of the large-scale motions.

In light of the foregoing argument, the QSH may be investigated upon a renormalisation of all statistical properties by reference to the local friction velocity:

$$\overline{X_i}|^{+,LS}_{Cf_{LS}} = \overline{X_i}|^{+}_{Cf_{LS}} \times u_\tau / u_{\tau,LS} \tag{8}$$

$$\overline{x_i' x_j'}|^{+,LS}_{Cf_{LS}} = \overline{x_i' x_j'}|^{+}_{Cf_{LS}} \times (u_\tau / u_{\tau,LS})^2 \tag{9}$$

$$y^+_{LS} = y^+ \times u_{\tau,LS} / u_\tau \tag{10}$$

Thus, when any of the properties is displayed as a map in the $y^+_{LS} - Cf_{LS}$ maps, homogeneity in the contours along the Cf_{LS} axis can be taken to signify the validity of the QSH.

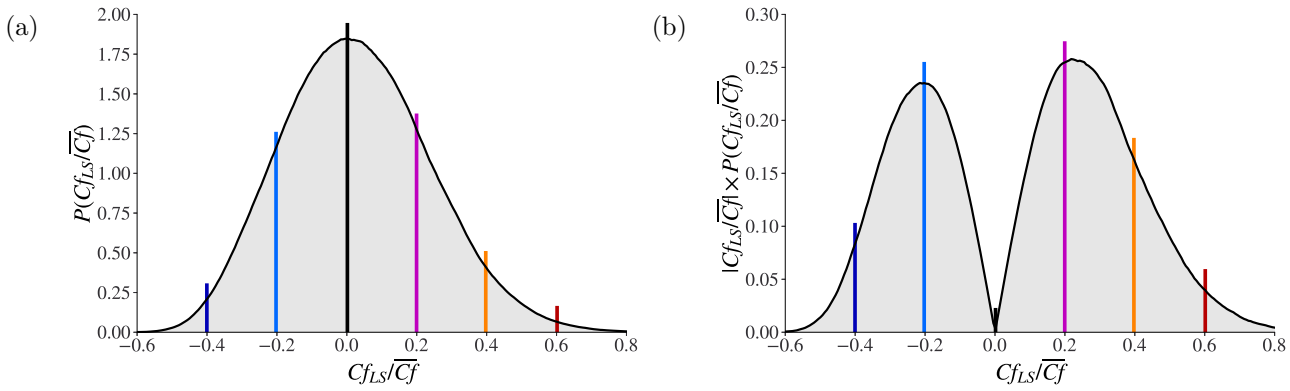

FIG. 7: PDF of the large-scale skin-friction fluctuations; (a) *pdf* with specific Cf_{LS} at which profiles of statistical properties are given in figures to follow; (b) PDF premultiplied by $|Cf_{LS}/\overline{Cf}|$ to accentuate the positive skewness.

IV. AMPLITUDE MODULATION AND MECHANISMS

Although the phenomenon of amplitude modulation has received considerable attention over the years, in a variety of studies published by a number of groups, a study of particular relevance in the present context is that of Agostini and Leschziner [22, 25]. One reason is that the statistical framework applied herein, as explained in Section III, was first put forward in that paper and used to examine modulation in channel flow at $Re_\tau \approx 1000$. More to the point, however, is the fact that Agostini and Leschziner [22, 25] were able to identify, arguably beyond doubt, that the modulation is provoked by large-scale-induced fluctuations in turbulence production associated with concurrent strain and shear-stress fluctuations, the strain fluctuations accompanying large-scale ejections, sweeps and quasi-streamwise vortices. It is natural, therefore, to examine the present flow, which is not only at a much higher Reynolds number, but in which the large-scale/small-scale decomposition is based in an entirely different strategy, relative to the EMD of Agostini and Leschziner [22, 25]. As many of the physical interactions are discussed in considerable detail in these studies, the present section restricts itself to discussing some essential results that are argued to demonstrate consistency and compliance with the earlier observations. As will transpire below, the essential message is that all conditional properties – stress components and production – respond in unison to the large-scale fluctuations, due to the conditional strain-rate

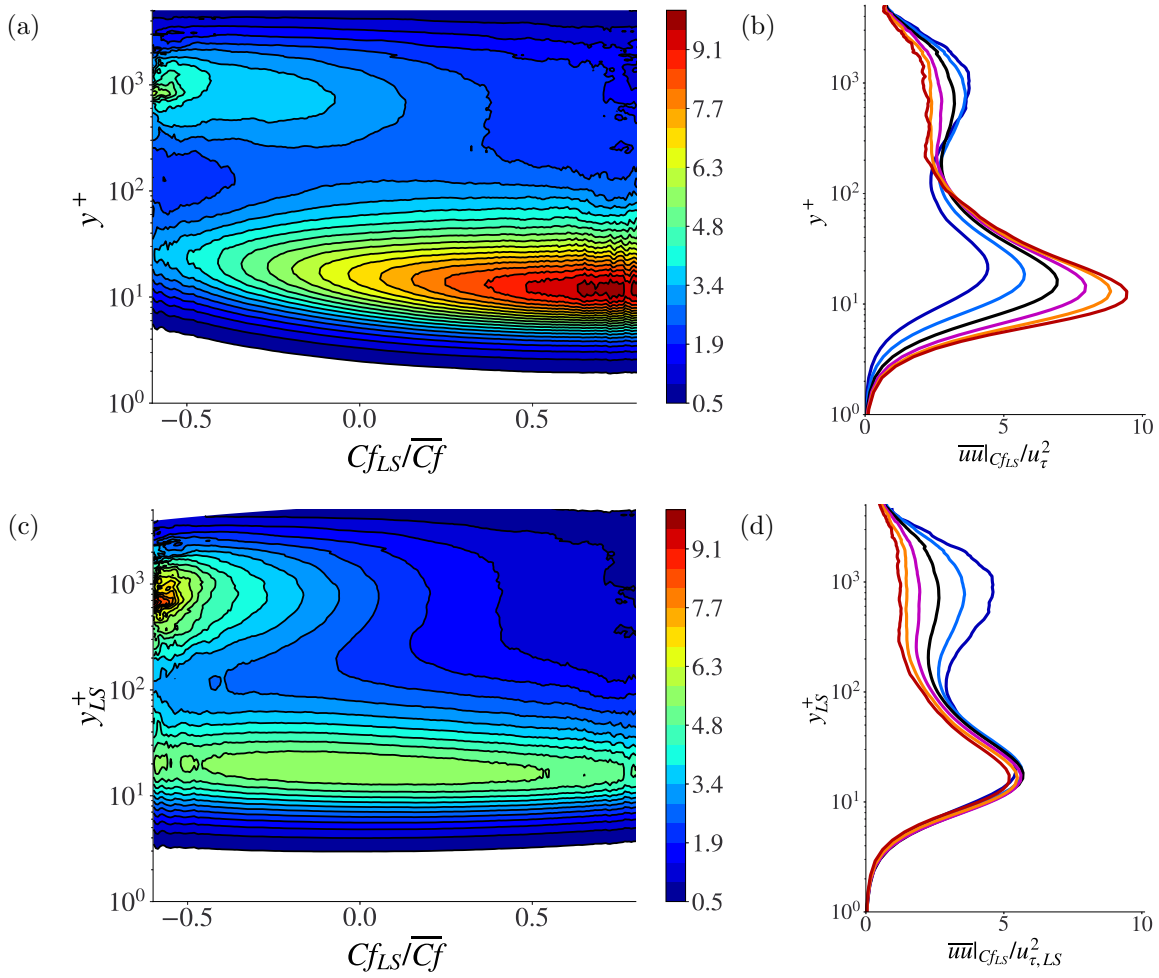

FIG. 8: Conditional response of the streamwise energy to the large-scale skin friction Cf_{LS}; (a) contours of conditional energy; (b) Profiles of conditional energy at locations marked on the inserted PDF; (c) contours in (a) re-scaled according to eqs.(8)-(10); (d) profiles in (b) re-scaled according to eqs. (8)-(10).

fluctuations driving the stress productions, and hence the stresses themselves, in the same direction.

The most obvious manifestation of modulation is the amplification and attenuation of the streamwise energy – although the spanwise and wall-normal components also give clear evidence of modulation, as demonstrated by Agostini and Leschziner [22, 25]. The response of the streamwise energy is conveyed in four ways: first, figures 8a, 8b show contour plots and profiles for the total (small-scale + large-scale components), respectively; second, figures 8c, 8d examine the validity of the quasi-steady hypothesis by way of the results in figures 8a,

8b being recast according to equations (8)-(10); third, figures 9a, 9b pertain to the response of the small-scale energy component only to the large scales; and forth. 9c, 9d corresponding to figures 8c, 8d, expose the validity of the quasi-steady hypothesis for the small-scale energy only. The profiles are given at the six values of Cf_{LS} marked in the PDF $P(Cf_{LS})$ given in figure 7. The latter shows the PDF to be positively skewed, which implies the tendency for large positive footprints to dominate over large negative ones. A positive skewness, albeit more pronounced, was also observed when the empirical mode decomposition was used at $Re_\tau \approx 1000$.

Figures 8a, 8b expose the strong amplification and somewhat more moderate attenuation of the streamwise energy in the buffer layer for positive and negative footprints, respectively. In contrast, the energy in the outer layer is negatively correlated with the footprints. Both features are well-known, having been reported in previous studies for other flows. As noted already, and demonstrated below, this dependence reflects fluctuations in strain-induced turbulence generation. Figures 8c, 8d suggest, again in qualitative agreement with previous observations by Agostini and Leschziner [22, 25] for $Re_\tau \approx 1000$, that the quasi-steady hypothesis holds for the streamwise energy, but only in the viscosity-affected layer, up to $y^+ \approx 80$ within which the time scale of the small-scale motions is substantially shorter than that of the footprints.

With attention redirected to the results for the small-scale energy, in figure 9, it is observed first that the amplification and attenuation levels in the buffer layer are very similar to those of the total energy, figure 8, signifying the strong dominance of the small-scale energy component at the wall. However, in the outer region, the large scales dominate, and the sensitivity of the small-scale turbulence to the large scales is low. Again, in anticipation of what is to follow, it is remarked here that the behaviour both in the inner and outer layers is driven by conditional shear-strain fluctuations which are of opposite sign in the inner and outer layers for any given Cf_{LS} value.

The generative mechanism which is responsible for the modulation shown in figure 8 is clarified by way of the shear-stress profiles in figure 10 in conjunction with the streamwise-energy production in figure 11. The latter profiles are shown in two ways: the default form in 11a and the y^+-premultiplied form in 11b. The latter profiles accentuate the sensitivity in the outer layer in which actual production fluctuations are rather weak, but nevertheless clearly present. The shear-stress profiles demonstrate that the modulation of this stress

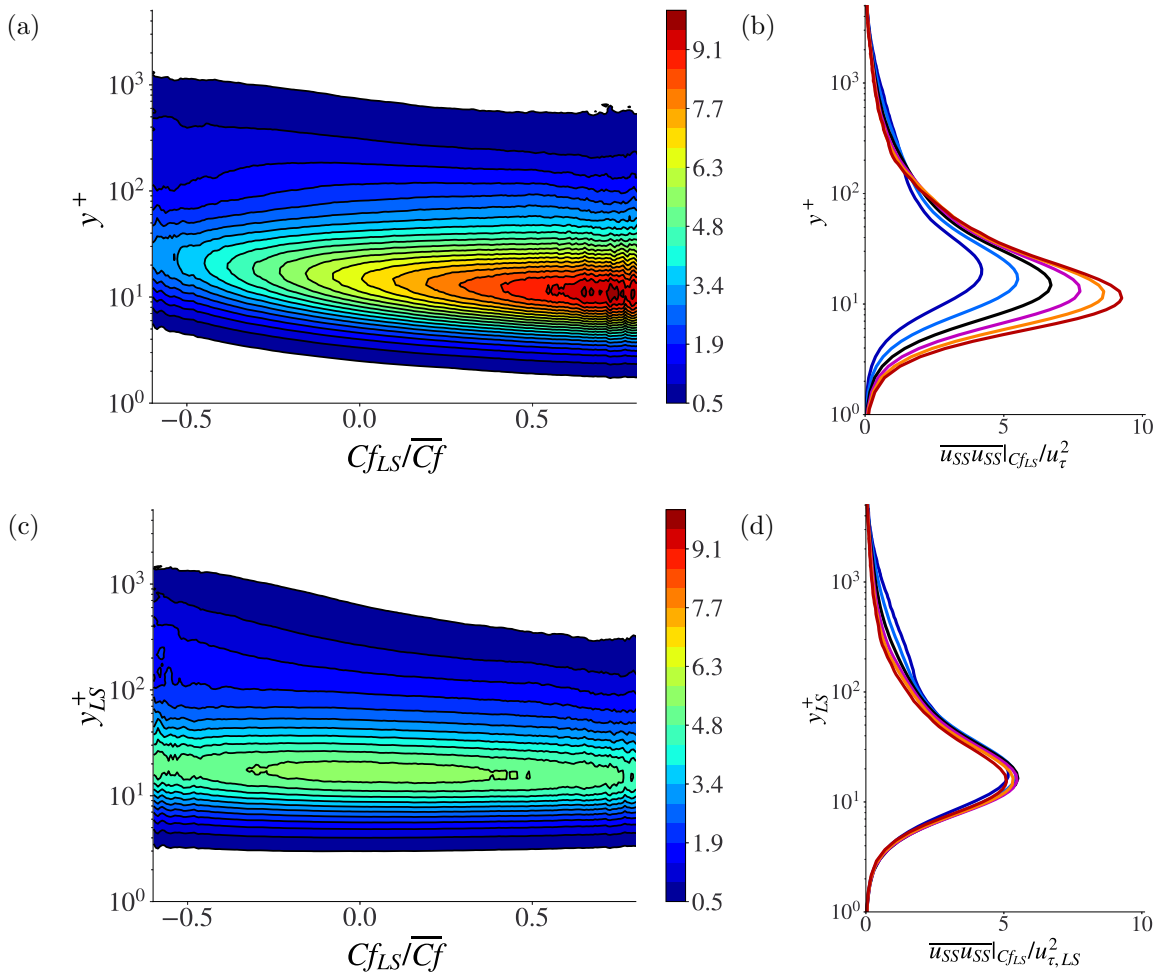

FIG. 9: Conditional response of the small-scale component of the streamwise energy to the large-scale skin friction Cf_{LS}; (a): contours of conditional energy; (b) profiles of conditional energy at locations marked on the inserted *pdf*; (c) contours in (a) re-scaled according to eqs. (8)-(10); (d) profiles in (b) re-scaled according to eqs. (8)-(10).

follows closely that of the streamwise energy. The fact that the production also follows the same trends is due to the perturbations in the conditional shear strain (not included here, but demonstrated in [22, 25]) being aligned with those of the shear stress: the near-wall strain steepens for positive Cf_{LS} and weakens for negative values, the reverse occurring in the outer layer. These strain fluctuations go hand-in-hand with large-scale sweeps, for positive Cf_{LS} values, and ejections for negative values. While profiles of the shear-stress production are not included herein, it is noted that these too follow similar tends as the streamwise-stress production, because the wall-normal stress is also modulated in a manner

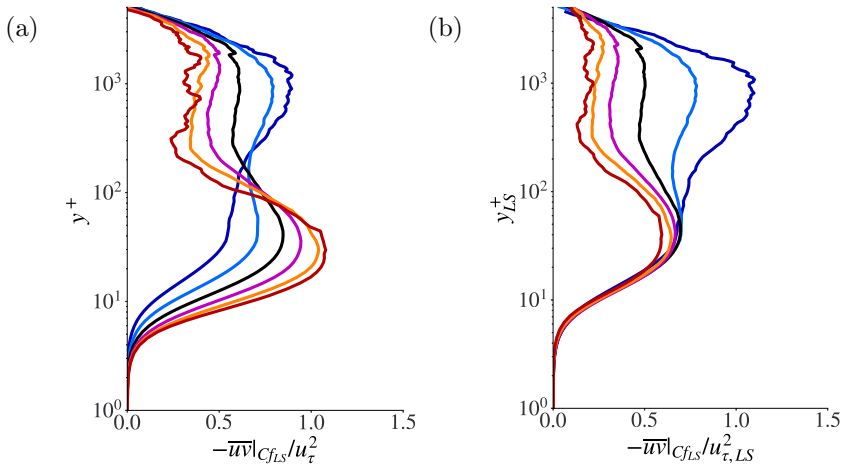

FIG. 10: Conditional response of the shear-stress energy to the large-scale skin friction Cf_{LS}; (a) Profiles of conditional stress at locations marked in figure 7; (b) profiles in (a) re-scaled according to eqs. (8)-(10).

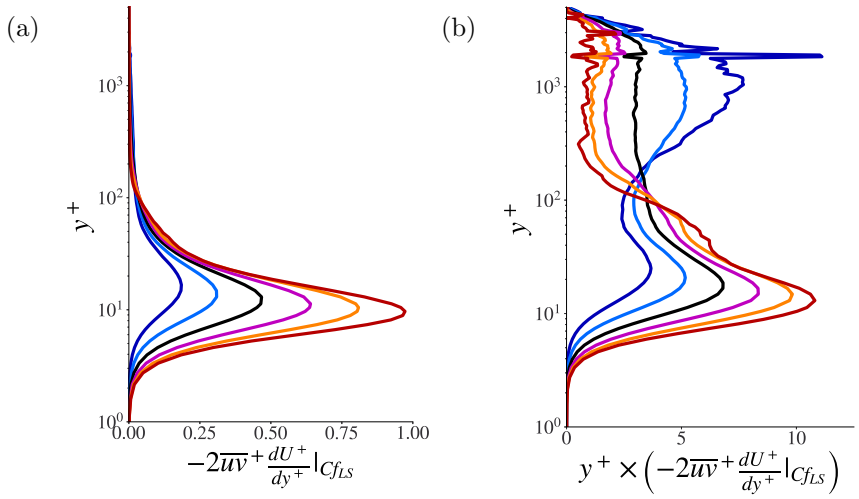

FIG. 11: Conditional response of the production of the streamwise energy component to the large-scale skin friction: (a) profiles of conditional production at locations marked in figure 7; (b) profiles in (a) premultiplied by y^+.

analogous to that of the other stress components. This includes the spanwise stress, profiles of which are given in figure 12. While the production of this stress is zero, of course, the pressure-strain-interaction mechanism transfers energy from the streamwise to the spanwise stress component, thus causing a rise and fall in the near-wall stress alongside corresponding

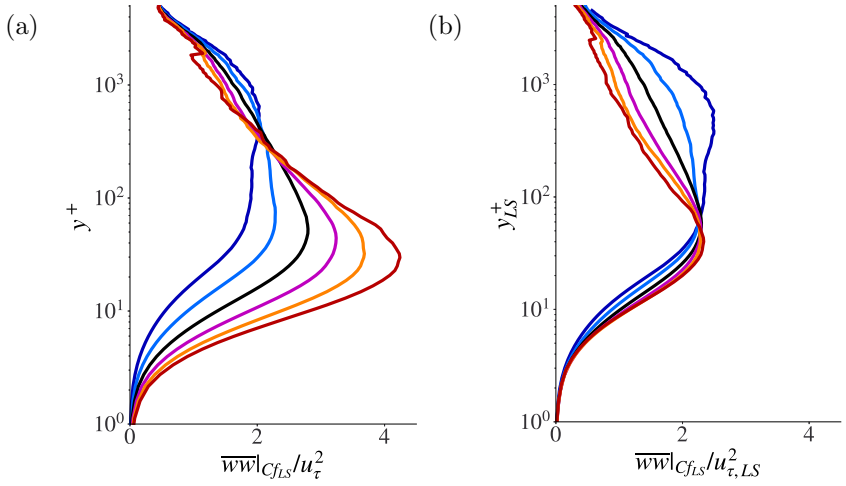

FIG. 12: Conditional response of the spanwise energy to the large-scale skin friction Cf_{LS}; (a): profiles of conditional stress at locations marked in figure 7; (b): profiles in (a) re-scaled according to eqs. (8)-(10).

variations in the streamwise stress. The shear stress is seen to comply with the quasi-steady hypothesis, albeit over a reduced wall distance relative to the streamwise stress. Adherence of the spanwise stress with the quasi-steady hypothesis is markedly worse, however, and this departure has also been observed by Agostini and Leschziner [22] in their study of channel flow at $Re_\tau \approx 1000$. In that paper, the authors discuss in some detail (see figures 7 and 8 in that paper) the role of wall "splatting" provoked by large-scale sweeps on the near-wall behaviour of the spanwise stress. In particular, sweep-induced splatting causes a substantial strengthening of the spanwise fluctuations close to the wall, which partially decouples this stress from the processes governing the streamwise fluctuations and thus also from the associated universal scaling with the large-scale streamwise wall shear stress. A possible contributory reason for the indifferent behaviour shown in figure 12b is a time lag between the elevation of the turbulence intensity by production and the transfer of some of that energy to the spanwise stress, thus likely to weaken the universality of the scaling of this stress with the large-scale wall shear stress.

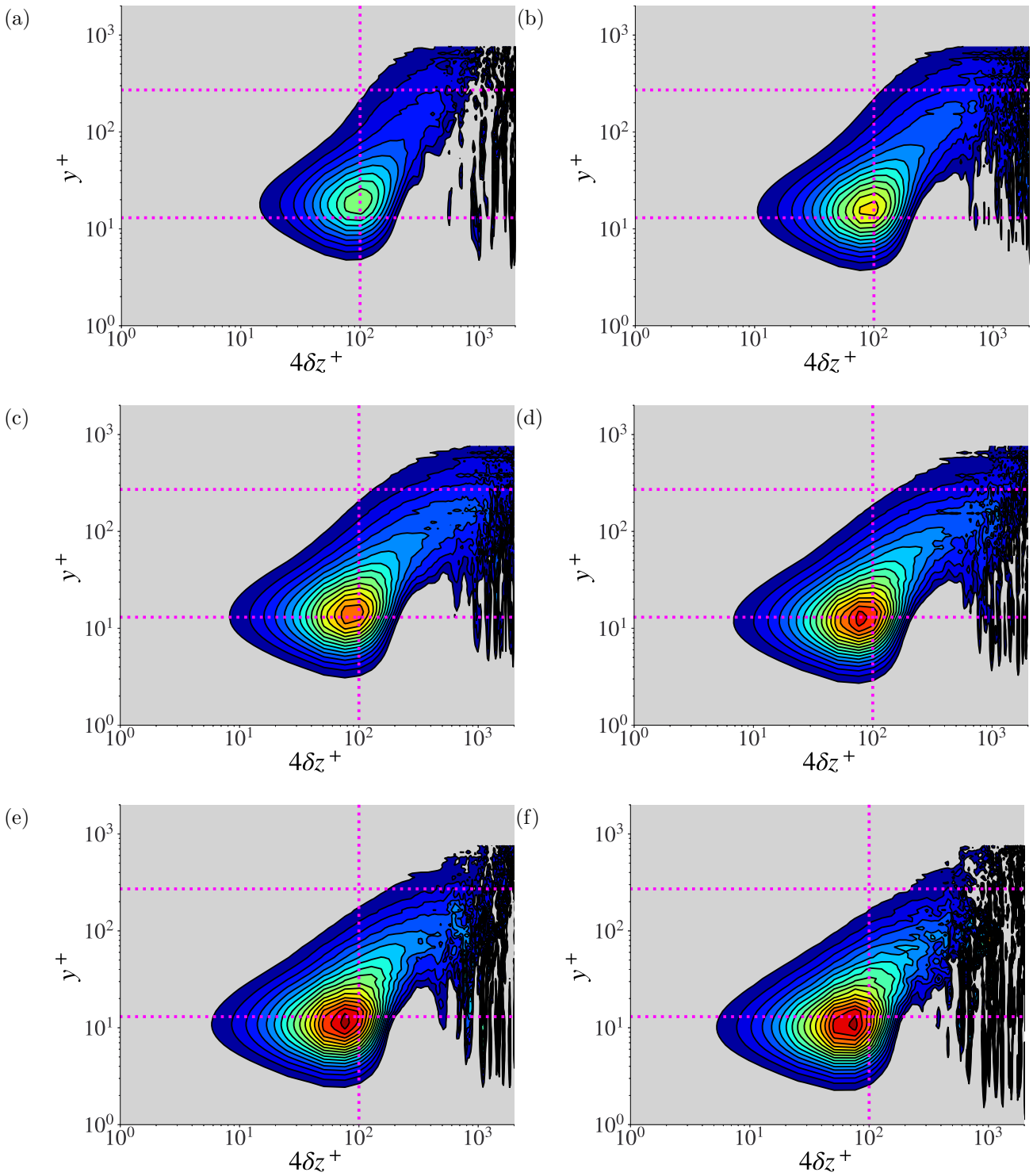

FIG. 13: Maps of $\delta z \frac{dS_u^2(\delta z)}{d\delta z}|^+_{Cf_{LS}}$ in the $y^+ - \delta z^+$ plane conditional on the six Cf_{LS} shown in figure 7; (a)-(f) arranged in order of rising Cf_{LS} values.

V. LENGTH-SCALE MODULATION

Figure 13 shows six maps of the premultiplied derivative of the second-order structure function in the $\delta z^+ - y+$ plane at the 6 conditional values of Cf_{LS} shown in the *pdf* of figure 7. Attention is first drawn the choice of the abscissa: $4\delta z^+$. The choice of this multiplier is rooted in the correspondence between the derivative of the structure function and the spectra, an equivalence demonstrated and discussed in Agostini and Leschziner [45] and shown in figure 6. In the latter, the abscissa is conventionally the wave length λ_z^+. Multiplying δz^+ by 4 is observed to shift the peak in the map at $y^+ = 12$ and $Cf_{LS} = 0$ to the value to $4\delta z^+ \approx 100$, corresponding to $\lambda_z^+ \approx 100$ – i.e., the accepted level of the spanwise separation distance between streaks as derived from two-point correlations.

There are three observations that can now be made by reference to figure 13. First, as Cf_{LS} increases, there is a progressive shift of the maximum towards the wall. This process and the mechanisms responsible have been discussed in detail in Agostini and Leschziner [25]. In essence, large positive Cf_{LS} levels cause a steepening of the strain close to the wall, thus generating increased small-scale turbulence and thinning the viscous sublayer. More interesting in the present context is that the increase in Cf_{LS} is also accompanied by a progressive reduction in the length-scale maximum from $4\delta z^+ \approx 100$ to around 65, which may be interpreted as indicating the length-scale modulation. The third feature deserved to be highlighted is the progressive widening of the scale spectra around the buffer layer for increasing Cf_{LS}. This widening appears to be due primarily to a shift of the range of short length scales towards lower values, a process especially noticeable when tracking the left-most edge of the spectra at $y^+ \approx 10$. In contrast, the longer scales around the buffer layer, at $4\delta z^+ \approx 200$, experience no discernible shift (the downward-pointing tongues at $4\delta z^+ > 1000$ signify the footprinting process). The increased predominance of small scales with increasing Cf_{LS} will be revisited later in the context of discussing the applicability of the QSH to the length-scale modulation.

The length-scale reduction is well brought out in figure 14, which shows contours of the premultiplied gradient of the second-order structure function in the Cf_{LS}-δz^+ plane, derived by taking, for each value of Cf_{LS} (many more than included in figure 13), δz^+-wise cuts at levels y^+ at which the peaks of the derivative arise. The black line is thus the locus of the peak of the gradient across the Cf_{LS} range. This corresponds almost identically to

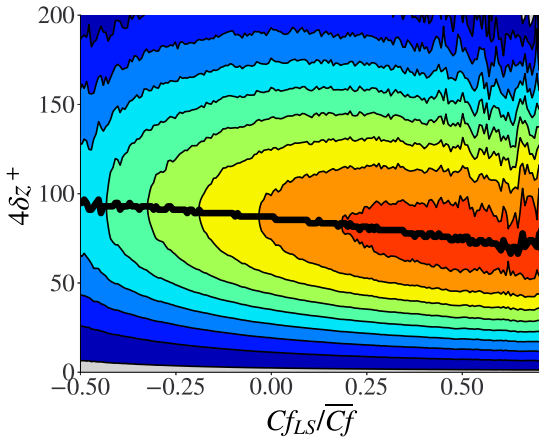

FIG. 14: Map of $\delta z \frac{dS_u^2(\delta z)}{d\delta z}|^+_{Cf_{LS}}$ in the $\delta z^+ - Cf^+_{LS}$ plane at $y^+ \approx 13$. The black line is the locus of maximum conditional value of the premultiplied derivative, demonstrating the reduction in wavelength with Cf_{LS}.

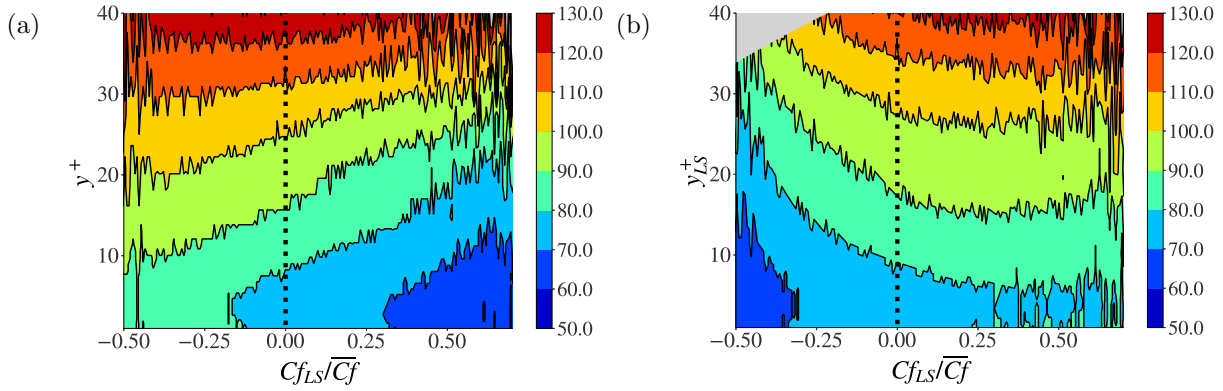

FIG. 15: Maps of conditional $4\delta z^+|_{Cf_{LS}}$ in the $y^+ - Cf_{LS}$ plane derived from $\delta z \frac{dS_u^2(\delta z)}{d\delta z}|^+_{Cf_{LS}}$ (for streamwise fluctuations); (a) nominal field scaled with mean wall shear stress; (b) field in (a) rescaled with large-scale wall shear stress (eq. (10)) to demonstrate adherence to the quasi-steady hypothesis.

the location $y^+ \approx 13$, scaled with the mean wall shear stress. As seen, the length scale for the location of the peak value in $\delta z \frac{dS_u^2(\delta z)}{d\delta z}|^+_{Cf_{LS}}$ reduces from around 100 at high negative large-scale fluctuations to around 65 at the highest large-scale fluctuations.

To examine whether the QSH applies to the length-scale modulation, a map of contours of the wave length corresponding to the maximum value of the derivative of the structure

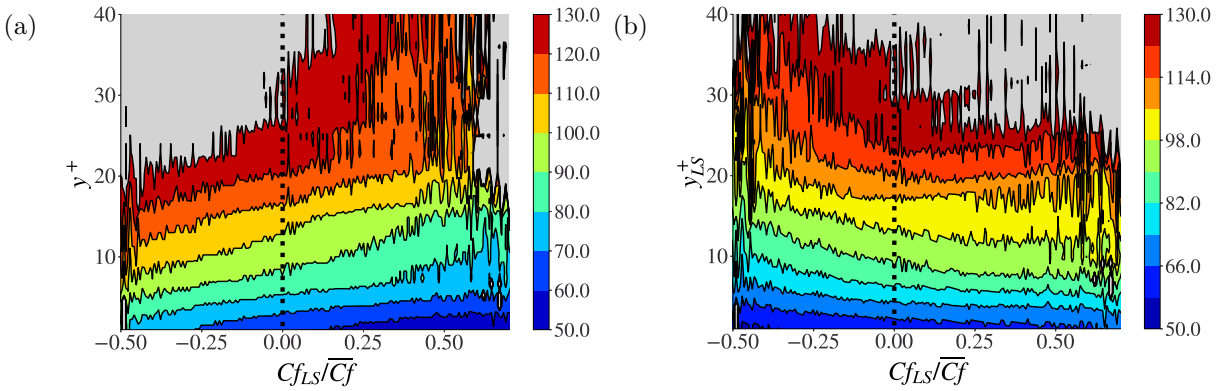

FIG. 16: Maps of conditional $4\delta z^+|_{Cf_{LS}}$ in the $y^+ - Cf_{LS}$ plane derived from $\delta z \frac{dS_w^2(\delta z)}{d\delta z}|^+_{Cf_{LS}}$ (for spanwise fluctuations) ; (a) nominal field scaled with mean wall shear stress; (b) field in (a) rescaled with large-scale wall shear stress (eq. (10)) to demonstrate adherence to the quasi-steady hypothesis.

function at different y^+ values and conditional on Cf_{LS} is derived. This is shown in figure 15a. The map demonstrates that the wave length of the maximum derivative location at any given y^+ is decreasing, as already observed by reference to Figures 13 and 14. For example, at $y^+ \approx 13$, the wave length in figure 15a is seen to decline from 100 (green shade) to around 70 (dark blue shade), which is clearly consistent with the black line in figure 14. Next, the map in figure 15a is re-scaled with the wall-normal distance and the wave length normalised with the large-scale wall shear stress, in accordance with equation (10) and $\delta z^{+,LS} = \delta z^+ \times u_{\tau,LS}/u_\tau$. This yields the map given in figure 15b, which permits two major observations to be made. First, the contours are broadly horizontal in the positive range of Cf_{LS}, implying that the QSH applies to frequency modulations of the fluctuations within the near-wall layer, $y^+ < 40$. Second, the hypothesis is not satisfied for negative large-scale fluctuations. As the length-scale modulation is here considered within the confines of the near-wall layer, up to y^+ of approximately 40, the lack of of adherence of length-scale fluctuations with the QSH at negative Cf_{LS} is inconsistent with the behaviour observed in respect of the amplitude modulation. Similar observations can be made in respect of the maps shown in figure 16 for the structure function S_w^2 – i.e., those pertaining to the spanwise fluctuations, which also show a limited correspondence to the quasi-steady hypothesis.

It can be argued that there is no compelling reason for why amplitude and length-scale

modulation should strictly go hand-in-hand. A possible, albeit somewhat tentative, interpretation of the behaviour in figures 15 and 16 starts from the observation that the width of the spectra of scales in figure 13 is narrowing at negative Cf_{LS} and broadening for positive Cf_{LS}. As observed earlier, by reference to figure 14, the predominant feature of the broadening spectrum to Cf_{LS} is a shift of the length-scale range towards lower values. It is recalled that the conditional energy and shear strain increase for positive Cf_{LS} and decrease for negative values, with the conditional strain and the velocity itself following suit. It is reasonable to argue, therefore, that the likely response of the spectra to this increase and decrease is the observed shift of the small-scale end of the scale spectra towards or away from low values, respectively. In fact, this shift has already been highlighted earlier when the spectra in figure 13 were discussed. A shift towards smaller scales will favour the QSH, while a greater prevalence of larger scales will prejudice the hypothesis. Figure 15a indeed shows a continuous decline in the length scale across the entire range of Cf_{LS}. The fact is, however, that the large-scale shear stress in the negative Cf_{LS} range increases at a faster rate than the rate at which the length scale drops, which then results in the violation of the QSH in the left-hand-side part of figure 15b. Here, the objection might be raised that the same does not apply to the stress components (except perhaps ww^+). However, it is reasonable to assume that velocity fluctuations are more closely tied to (and are more akin to) the shear velocity than is the length scale. Hence, it is not entirely surprising to observe differences in the level of adherence to the hypothesis for physically different types of statistical properties.

VI. DISCUSSION

Although the principal objective of the paper is to illuminate fundamental interactions that do not necessarily have any practical implications, the question might justifiably be posed as to what potentially useful messages can be taken forward into the domain of flow and turbulence control. The discussion below aims to answer this question.

A significant practical aspect of the study pertains to the mechanisms by which the turbulent drag is affected by outer structures and the manner in which these mechanisms interact with drag-reducing control methods. These issues have previously been addressed in previous studies [25, 27, 47], the last two in the context of drag reduction by transverse

oscillatory wall motions, but in all cases at the much lower Reynolds number, $Re_\tau \approx 1000$, than in the present study. One key mechanism is the amplification of turbulence in the buffer layer provoked by large-scale sweeps, and hence a strengthening of the streaks and an increase in the drag. These sweeps are correlated with positive large-scale skin-friction fluctuations, and they cause an increase in near-wall turbulence production, all part and parcel of the modulation process. While large-scale ejections, associated with negative large-scale skin-friction fluctuations, lead to a decline in near-wall turbulence, Agostini & Leschziner [25, 47] show this part of the modulation to be weaker, the asymmetry in the process being especially pronounced in the case of drag-reducing transverse wall motion. Previous studies investigated channel flows at $Re_\tau \approx 1000$ using the EMD. The present study, adopting the AE scale-separation methodology, shows that the same mechanisms prevail at the much higher Reynolds number – although, here, the flow is canonical rather than being actuated, in which case the asymmetry in the attenuation and amplification elements of the modulation is modest. Several studies [28, 30, 48] show that the drag- reduction effectiveness of oscillatory wall motion declines with Reynolds number, and this provides strong motivation for studying the modulation mechanisms at high Reynolds numbers. If the degradation in drag-reduction effectiveness is indeed rooted in the streak strength responding to the large-scale motions provoked by the outer structures, it follows that the design of control strategies, capable of providing substantial drag reduction at higher Reynolds numbers, has to rely on understanding the alteration of the small scale near-wall turbulence, in terms of both magnitude and length/time scales, by the outer structures. This understanding is aided by the present results.

Another area to which the present study relates is the predictive modelling of modulation by the use of correlations that link the intensity of the modulation in the inner region to the large-scale outer fluctuations and the footprints. Since the introduction of the notions of "footprint" and "modulation" by Marusic *et al.* [49], there have been numerous articles on how to improve the predictive model they introduce, and a great deal of effort has been devoted to defining the empirical parameters in the model. Marusic *et al*'s model was derived by reference to experimental observations. In contrast, Chernyshenko *et al.* [23, 50] have introduced an elegant new theory based on the hypothesis that the near-wall statistics follows the universal "law of wall" if scaled by the large-scale local skin friction, rather than the mean value. Upon validating this theory, wall-bounded flow can then be accurately

predicted up to upper part of the buffer layer by only using the footprints of the large-scale outer structure and an universal canonical signal. The present paper examines the validity of the quasi-steady theory and shows that, in respect of turbulence velocity statistics, the theory applies only in the near-wall region, roughly up to $y^+ \approx 80 - 100$. In contrast, the theory is shown herein to extend only in a very restricted sense to the length-scale modulation. The modulation models discussed above are restricted to streamwise fluctuations and streamwise turbulence intensity only. As the EMD- and AE-based scale-resolving methods yield the full spatial field of the large-scale skin friction and the fully three-dimensional field of the associated large-scale motions, conditional on the skin-friction magnitude, this capability opens the way to extending the conventional models to the modulation in the spanwise direction. This may not be regarded as an especially fruitful or interesting proposition, because the drag normal to the flow direction is rarely of interest. Moreover, the present study shows that the quasi-steady hypothesis for the spanwise near-wall intensity is less well satisfied than that of the streamwise intensity. However, one aspect that could be of interest is the provision of information on the large-scale quasi-streamwise vortices, with the objective of relating the rotational motions to any drag enhancement that is connected to the momentum mixing caused by the large-scale vortices. This is one area that may be explored further in future studies in future studies.

VII. CONCLUSIONS

This study combined a joint, multiple-variable joint-PDF methodology with two entirely novel elements – a decoder-encoder-based scale-decomposition technique and the conditional derivative of the structure function — for the purpose of analysing the response of the near-wall layer in a turbulent channel flow at $Re_\tau \approx 5200$ to energetic large-scale outer structures in the log-layer. The joint-PDF technique, previously used to examine amplitude modulation in channel flow at $Re_\tau \approx 1000$, is here applied to channel flow at a much higher Reynolds number by processing full-volume DNS realisations generated by Lee and Moser [33]. The structure function, derived by sampling the DNS data conditionally on large-scale skin-friction footprints, is used to investigate the modulation of the length scale in the near-wall layer. The main conclusions can be summarised as follows:

- As is conveyed by the conceptual sketch in figure 17, the overarching conclusion of the

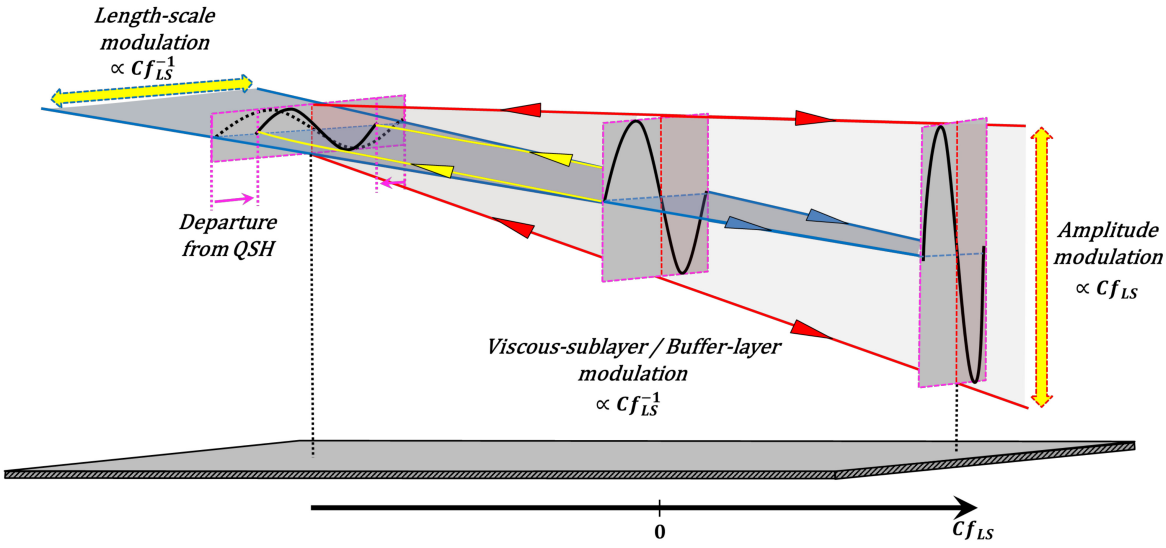

FIG. 17: Conceptual representation of the modulation of the near-wall turbulence induced by outer large-scale motions as predicted by the Quasi-Steady Hypothesis. Modulation closely in portion with Cf_{LS} indicates adherence to QSH and represented by straight diverging red and converging blue lines. Departure of length-scale modulation from QSH for negative Cf_{LS} indicated by curved yellow lines.

study is that the modulation of the energy around the buffer layer rises in proportion to the large-scale skin friction Cf_{LS}, while the length scale modulation declines at a similar rate.

- The amplitude modulation of the stresses follows, qualitatively, that observed previously for $Re_\tau \approx 1000$, but is more intense and more pronounced.

- The conditional streamwise stress in the buffer layer varies within the range of approximately 70% of the mean over the range of the skin-friction footprints. Similar variations arise in the conditional shear stress and the spanwise energy. In all stress components, the levels are amplified for positive large-scale skin-friction fluctuations and are attenuated for negative ones. These variations are governed primarily by the response of the small-scale components to the footprints – i.e., sweeps and ejections produced by the outer large-scale structures.

- The response of the conditional stresses in the outer layer is negatively correlated with the footprints — i.e., their response is opposite to that of the near-wall stresses. In this layer, the large-sale components dominate over the small-scale ones, and thus the modulation is primarily a reflection of the role of the large-scale stresses.

- The generation rate of the streamwise energy varies in harmony with the stress components — i.e., the generation is positively correlated with the large-scale footprints in the buffer layer, while they are negatively correlated in the outer layer. This is entirely in accord with previous observations and strengthens the conclusion that the modulation is a consequence of the conditional production being driven by large-scale sweeps and ejections, the former provoking buffer-layer implication and the latter outer-layer amplification.

- Rescaling the conditional stresses, production and wall-normal distance with the large-scale wall shear stress is shown to support the quasi-steady hypothesis, but the validity of the hypothesis is confined to the near-wall layer, $y^+ < 80$. Adherence of the spanwise energy to the quasi-steady hypothesis is rather less good than that of the streamwise and shear-stress components, and this is attributed to distortions associated with sweep-induced "splatting" (flattening the structures) at the wall, and with the time lag between the production and the redistribution (pressure-strain) process.

- The modulation of the length scale is quantified primarily by examining the shift in the peak of the conditional derivative of the second-order structure function for the streamwise fluctuations in the buffer layer, at the location commensurate with that of the maximum energy density in the spectrum. This maximum is found to decrease progressively by about 40% across the range of the large-scale footprints. The shift in the maximum declines with increasing y^+ when judged by reference to the peak at that y^+ location. A qualitatively similar behaviour is observed in respect of the structure function for the spanwise fluctuations.

- Only a tentative interpretation of the length-scale modulation can be offered. This is based on the observation that the spectrum of scales widens with increasing Cf_{LS} values, thus increasing the content and contribution of smaller scales and hence also decreasing the length scale at the peak of the conditional derivative of the structure

function.

- The conditional length scale is found to adhere to the quasi-steady hypothesis only for positive large-scale footprints. In the negative range, the friction velocity declines faster than the rate at which the length scale increases, so that the length scale, when rescaled with the friction velocity of the footprints, is not constant across the Cf_{LS} range (a limitation indicated schematically by the broken yellow lines in figure 17). This is at variance with the behaviour observed in respect of the stresses, but there is no compelling physical reason to believe that both should go strictly hand-in-hand.

ACKNOWLEDGEMENTS

This work was partially supported by the French government program "Investissements d'Avenir" (EUR INTREE, reference ANR-18-EURE-0010).

AUTHOR DECLARATIONS

The authors have no conflicts to disclose

DATA STATEMENT

Data for the turbulent channel Flow at $Re_\tau = 5200$ that support the findings of this study are openly available at https://doi.org/10.7281/T1PV6HJV and are obtained from the JHTDB at http://turbulence.pha.jhu.edu

---

[1] N. Hutchins and I. Marusic, Evidence of very long meandering features in the logarithmic region of turbulent boundary layers, Journal of Fluid Mechanics **579**, 1 (2007).

[2] N. Hutchins and I. Marusic, Large-scale influences in near-wall turbulence, Philosophical Transactions of the Royal Society of London A: Mathematical, Physical and Engineering Sciences **365**, 647 (2007).

[3] R. Mathis, N. Hutchins, and I. Marusic, Large-scale amplitude modulation of the small-scale structures in turbulent boundary layers, Journal of Fluid Mechanics **628**, 311 (2009).

[4] C. E. Willert, J. Soria, M. Stanislas, J. Klinner, O. Amili, M. Eisfelder, C. Cuvier, G. Bellani, T. Fiorini, and A. Talamelli, Near-wall statistics of a turbulent pipe flow at shear reynolds numbers up to 40 000, Journal of Fluid Mechanics **826** (2017).

[5] T. Fiorini, G. Bellani, R. Örlü, A. Segalini, P. H. Alfredsson, and A. Talamelli, Turbulent pipe flow near-wall statistics, in *Progress in Turbulence VII* (Springer, 2017) pp. 89–94.

[6] A. J. Smits, B. J. McKeon, and I. Marusic, High-Reynolds number wall turbulence, Annual Review of Fluid Mechanics **43**, 353 (2011).

[7] A. Townsend, *The structure of turbulent shear flow* (Cambridge university press, 1980).

[8] R. Mathis, J. P. Monty, N. Hutchins, and I. Marusic, Comparison of large-scale amplitude modulation in turbulent boundary layers, pipes, and channel flows, Physics of Fluids **21**, 111703 (2009).

[9] B. Ganapathisubramani, N. Hutchins, J. Monty, D. Chung, and I. Marusic, Amplitude and frequency modulation in wall turbulence, Journal of Fluid Mechanics **712**, 61 (2012).

[10] W. Baars, K. Talluru, N. Hutchins, and I. Marusic, Wavelet analysis of wall turbulence to study large-scale modulation of small scales, Experiments in Fluids **56**, 1 (2015).

[11] G. Pathikonda and K. T. Christensen, Investigation of inner-outer interactions in a turbulent boundary layer using high-speed particle image velocimetry, Physical Review Fluids **4**, 034607 (2019).

[12] G. Iacobello, L. Ridolfi, and S. Scarsoglio, Large-to-small scale frequency modulation analysis in wall-bounded turbulence via visibility networks, Journal of Fluid Mechanics **918** (2021).

[13] P. Schlatter and R. örlü, Quantifying the interaction between large and small scales in wall-bounded turbulent flows: A note of caution, Physics of Fluids **22**, 051704 (2010).

[14] I. Jacobi and B. McKeon, Phase relationships between large and small scales in the turbulent boundary layer, Experiments in fluids **54**, 1 (2013).

[15] S. Duvvuri and B. McKeon, Triadic scale interactions in a turbulent boundary layer, Journal of Fluid Mechanics **767**, R4 (2015).

[16] D. Chung and B. McKeon, Large-eddy simulation of large-scale structures in long channel flow, Journal of Fluid Mechanics **661**, 341 (2010).

[17] M. Bernardini and S. Pirozzoli, Inner/outer layer interactions in turbulent boundary layers: a refined measure for the large-scale amplitude modulation mechanism, Physics of Fluids **23**, 061701 (2011).

[18] G. Eitel-Amor, R. Örlü, and P. Schlatter, Simulation and validation of a spatially evolving turbulent boundary layer up to reθ= 8300, International Journal of Heat and Fluid Flow **47**, 57 (2014).

[19] L. Agostini, M. Leschziner, J. Poggie, N. Bisek, and D. Gaitonde, Multi-scale interactions in a compressible boundary layer, Journal of Turbulence **18**, 760 (2017).

[20] E. Dogan, R. Örlü, D. Gatti, R. Vinuesa, and P. Schlatter, Quantification of amplitude modulation in wall-bounded turbulence, Fluid Dynamics Research **51**, 011408 (2019).

[21] A. Andreolli, D. Gatti, R. Vinuesa, R. Örlü, and P. Schlatter, Effects of sweeps and ejections on amplitude modulation in a turbulent channel flow, arXiv preprint arXiv:2109.09486 (2021).

[22] L. Agostini and M. Leschziner, On the departure of near-wall turbulence from the quasi-steady state, Journal of Fluid Mechanics **871** (2019).

[23] S. Chernyshenko, Extension of qsqh theory of scale interaction in near-wall turbulence to all velocity components, Journal of Fluid Mechanics **916**, A52 (2021).

[24] L. Agostini and M. Leschziner, On the influence of outer large-scale structures on near-wall turbulence in channel flow, Physics of Fluids **26**, 075107 (2014).

[25] L. Agostini and M. Leschziner, The connection between the spectrum of turbulent scales and the skin-friction statistics in channel flow at $Re_\tau \approx 1000$, Journal of Fluid Mechanics **871**, 22 (2019).

[26] E. Touber and M. A. Leschziner, Near-wall streak modification by spanwise oscillatory wall motion and drag-reduction mechanisms, Journal of Fluid Mechanics **693**, 150 (2012).

[27] L. Agostini and M. Leschziner, Statistical analysis of outer large-scale/inner-layer interactions in channel flow subjected to oscillatory drag-reducing wall motion using a multiple-variable joint-probability-density function methodology, Journal of Fluid Mechanics **923** (2021).

[28] D. Gatti and M. Quadrio, Reynolds-number dependence of turbulent skin-friction drag reduction induced by spanwise forcing, Journal of Fluid Mechanics **802**, 553 (2016).

[29] P. Ricco, M. Skote, and M. A. Leschziner, A review of turbulent skin-friction drag reduction by near-wall transverse forcing, Progress in Aerospace Sciences **123**, 100713 (2021).

[30] H. Hurst and Y. Chung, The effect of Reynolds number on turbulent drag reduction by streamwise travelling waves, Journal of Fluid Mechanics **under consideration** (2013).

[31] T. Nickels, I. Marusic, S. Hafez, and M. Chong, Evidence of the k_1^{-1} law in a high-Reynolds-number turbulent boundary layer, Physical review letters **95**, 074501 (2005).

[32] L. Lacasa, B. Luque, F. Ballesteros, J. Luque, and J. C. Nuno, From time series to complex networks: The visibility graph, Proceedings of the National Academy of Sciences **105**, 4972 (2008).

[33] M. Lee and R. D. Moser, Direct numerical simulation of turbulent channel flow up to $\mathrm{Re}_\tau \approx 5200$, Journal of Fluid Mechanics **774**, 395 (2015).

[34] A. T. Mohan, N. Lubbers, D. Livescu, and M. Chertkov, Embedding hard physical constraints in neural network coarse-graining of 3d turbulence, arXiv preprint arXiv:2002.00021 (2020).

[35] R. Maulik, B. Lusch, and P. Balaprakash, Reduced-order modeling of advection-dominated systems with recurrent neural networks and convolutional autoencoders, Physics of Fluids **33**, 037106 (2021).

[36] L. Agostini, Exploration and prediction of fluid dynamical systems using auto-encoder technology, Physics of Fluids **32**, 067103 (2020).

[37] P. Vincent, H. Larochelle, I. Lajoie, Y. Bengio, P.-A. Manzagol, and L. Bottou, Stacked denoising autoencoders: Learning useful representations in a deep network with a local denoising criterion., Journal of machine learning research **11** (2010).

[38] C. Zhou and R. C. Paffenroth, Anomaly detection with robust deep autoencoders, in *Proceedings of the 23rd ACM SIGKDD international conference on knowledge discovery and data mining* (2017) pp. 665–674.

[39] L. Guastoni, A. Güemes, A. Ianiro, S. Discetti, P. Schlatter, H. Azizpour, and R. Vinuesa, Convolutional-network models to predict wall-bounded turbulence from wall quantities, Journal of Fluid Mechanics **928** (2021).

[40] E. Plaut, From principal subspaces to principal components with linear autoencoders, arXiv:1804.10253 (2018).

[41] T. Murata, K. Fukami, and K. Fukagata, Nonlinear mode decomposition with convolutional neural networks for fluid dynamics, Journal of Fluid Mechanics **882** (2020).

[42] D.-A. Clevert, T. Unterthiner, and S. Hochreiter, Fast and accurate deep network learning by exponential linear units (elus), arXiv preprint arXiv:1511.07289 (2015).

[43] The relevant code and trained model will be make available on request.

[44] P. Davidson, P.-A. Krogstad, T. Nickels, *et al.*, A refined interpretation of the logarithmic structure function law in wall layer turbulence, Physics of Fluids **18**, 5112 (2006).

[45] L. Agostini and M. Leschziner, Spectral analysis of near-wall turbulence in channel flow at $\mathrm{Re}_\tau = 4200$ with emphasis on the attached-eddy hypothesis, Phys. Rev. Fluids **2**, 014603 (2017).

[46] I. De Moortel, S. Munday, and A. W. Hood, Wavelet analysis: the effect of varying basic wavelet parameters, Solar Physics **222**, 203 (2004).

[47] L. Agostini and M. Leschziner, The impact of footprints of large-scale outer structures on the near-wall layer in the presence of drag-reducing spanwise wall motion, Flow, Turbulence and Combustion , 1 (2018).

[48] E. Touber and M. A. Leschziner, Near-wall streak modification by spanwise oscillatory wall motion and drag-reduction mechanisms, Journal of Fluid Mechanics **693**, 150 (2012).

[49] I. Marusic, R. Mathis, and N. Hutchins, Predictive model for wall-bounded turbulent flow, Science **329**, 193 (2010).

[50] S. Chernyshenko, I. Marusic, and R. Mathis, Quasi-steady description of modulation effects in wall turbulence, arXiv:1203.3714 [physics] (2012).